Stimulated Concentration Scattering in the Binary-Gas Mixtures Xe-He and SF_6-He†

W. H. Lowdermilk* and N. Bloembergen
Division of Engineering and Applied Physics, Harvard University, Cambridge, Massachusetts 02138
(Received 11 October 1971)

The frequency shift of the backscattered light, stimulated by an intense ruby-laser beam, has been measured in mixtures of 5 atm of SF_6 and 0–50 atm of He, and also in mixtures of 8 atm of Xe and 0–80 atm of He. For relative He concentrations less than 60%, the frequency is characteristic of stimulated Brillouin scattering. Above 60% He concentration, a rapid decrease in the frequency shift takes place characteristic of stimulated concentration scattering. Good agreement is obtained with the theory and also with recent data on spontaneous concentration scattering in the same gas mixtures.

I. INTRODUCTION

The possibility of observing stimulated concentration scattering was first suggested by Bespalov and Kubarev.[1] These authors claimed to have observed the phenomenon in a mixture of two liquids. Theoretical analysis[2] indicates that in their mixture the gain coefficient of the stimulated Brillouin effect should have been four or five orders of magnitude larger than the gain coefficient of stimulated concentration scattering. The small frequency shift observed may have been caused by stimulated thermal Rayleigh scattering.[3]

Careful consideration of the theory shows that it requires very special circumstances for the stimulated concentration gain to become comparable to, and therefore competitive with, other nonlinear processes, such as the stimulated Brillouin scattering, stimulated Raman scattering, stimulated Rayleigh wing scattering in the case of fluids with anisotropic molecules, and, in the case of absorbing media, stimulated thermal Rayleigh scattering.

The theory indicates[2] that the most favorable condition for observation of the stimulated concentration scattering occurs in a mixture of gases, in which the two constituent molecules have a large difference in mass and optical polarizability. The total pressure should be kept as low as possible, yet still be within the hydrodynamic regime. The reason is that the stimulated Brillouin gain increases as the square of the density in the gas, because the acoustic damping constant is inversely proportional to the density,[4] while the stimulated concentration gain increases only linearly with density.

The following simple physical picture may be helpful in comparing the two effects. Under the influence of the forward laser wave with electric field E_L and the backward Stokes-shifted wave E_S polarized parallel to E_L there will be volume elements in the fluid where E_L and E_S are in phase, and about a quarter wavelength away they will be 180° out of phase. Higher density of the gas tends to be created in the former regions, lower density in the latter, because the situation with a periodic density fluctuation has a lower dielectric free energy. This describes the electrostrictive coupling between the two light fields and the acoustic field. When the periodic density fluctuation is at resonance, a 90° phase shift, which is due to the sound wave damping, occurs in density amplitude with respect to the electrostrictive driving force. In this case the exponential gain of the wave E_S proportional to $|E_L|^2$ is a maximum. This parametric down conversion of a laser wave into a Brillouin-scattered wave and an acoustic wave is a well-known description of the stimulated Brillouin oscillator.

Consider now a binary gas mixture at constant total number density or constant total pressure. There will be a tendency for the relative concentration of the component with higher polarizability to be higher in volume elements where E_L and E_S are in phase and lower where they are 180° out of phase. This periodic variation in concentration would again tend to minimize the dielectric free energy. Thus a coupling of the two light waves and the concentration mode exists. The latter has a diffusive character and its dispersion relation is, of course, quite different from the acoustical dispersion relation. The necessary phase shift for exponential gain is provided by the diffusion process, and maximum gain results for a frequency shift $\Delta\omega_c = Dk^2$, where D is the diffusion constant and $\vec{k} = \vec{k}_L - \vec{k}_S$ is the scattering vector. A large difference in polarizability of the two types of molecules is obviously required to make the coupling to the concentration mode strong. A large difference in mass is required to provide extra damping for the acoustic mode. The increase in damping is basically caused by the different rate of thermalization of the light and heavy component in the mixture.

On the basis of these physical considerations, one of the best candidates for observing stimulated concentration scattering would be a mixture of xenon and helium. Raman and Rayleigh scattering are

absent. Indeed, Aref'ev and Morozov[5] reported the observation of stimulated concentration scattering, simultaneously with stimulated Brillouin scattering, in a mixture of 2.7–3.6 atm of He and 0.3–0.4 atm of Xe. The effect could only be observed at such high-power flux densities that a breakdown electric discharge was observed at the same time. It is known that numerous other nonlinear processes may occur during a breakdown, and small frequency shifts of stimulated scattered light, possibly caused by thermal Rayleigh scattering associated with plasma heating, have been observed during breakdown in pure noble gases.[6] Furthermore, the stimulated concentration effect was not observed when the total pressure was raised above 4 atm. These observations are not in agreement with the predictions of a quantitative theory of stimulated concentration scattering. Therefore the results of Aref'ev and Morozov cannot be regarded as conclusive.

When their results were published, our experiments on a mixture of SF_6 and He were in progress. We succeeded in demonstrating the shift in frequency of the stimulated backscattered light quantitatively[7] as a function of the He concentration in a mixture containing a partial pressure of 5 atm of SF_6. An abrupt decrease in the Stokes shift was observed when the partial pressure of He exceeded 60% of the total pressure. This effect was observed while electric breakdown of the gas was avoided. The preliminary results were in good agreement with theoretical expectations.[2,7] We have subsequently extended our observations to higher partial pressures of SF_6 and also to He-Xe mixtures. In the meantime, spontaneous concentration scattering data on these same binary gas mixtures have been obtained, the theoretical analysis has been refined, and excellent agreement between theory and experiment now exists. It is shown that the coupled hydrodynamic equations for density, temperature, and relative concentration must be solved exactly. The approximation of an isolated acoustic (Brillouin) mode and a Rayleigh mode is not sufficiently accurate. In the case of strong damping the concentration and density fluctuations may not be treated independently. They become effectively coupled. In Sec. II of this paper, the results of more refined calculations of the previously described hydrodynamic theory of stimulated scattering[2] will be presented. In Sec. III the experimental arrangement and procedure will be described in detail, while in Sec. IV the definitive experimental results on stimulated scattering in He-Xe and He-SF_6 mixtures will be presented and compared with theory.

II. HYDRODYNAMIC THEORY OF STIMULATED SCATTERING IN BINARY GAS MIXTURES

The coupling between the density, temperature, and relative concentration in a binary gas mixture in the hydrodynamic regime may be found in standard textbooks on fluid mechanics.[8] In the presence of an electric field $E = E_L + E_S$ resulting from the presence of two light waves, the differential free energy per unit mass must be augmented by terms representing variations in the light fields and variations in the dielectric constant:

$$dF = -s_0\,dT + \mu_0\,dc + \frac{P_0}{\rho^2}\,d\rho - \frac{\epsilon E\,dE}{4\pi\rho} - \frac{E^2\,d\epsilon}{8\pi\rho}, \quad (1)$$

where s_0, μ_0, and P_0 are the entropy, chemical potential, and pressure, respectively, when the electric field is absent. Here ϵ must be regarded as a function of the variables T, c, ρ. It can be shown that the force per unit volume on an uncharged dielectric is increased in the presence of an electric field by an amount[9]

$$\frac{\rho}{8\pi}\,\mathrm{grad}\left[E^2\left(\frac{\partial\epsilon}{\partial\rho}\right)_{T,c}\right] - \frac{E^2}{8\pi}\left(\frac{\partial\epsilon}{\partial T}\right)_{\rho,c}\mathrm{grad}\,T - \frac{E^2}{8\pi}\left(\frac{\partial\epsilon}{\partial c}\right)_{T,\rho}\mathrm{grad}\,c\,.$$

The last two terms are usually negligible compared to the first term. The effect of electrostriction is therefore to add a term

$$\frac{1}{8\pi}\left[E^2\left(\frac{\partial\epsilon}{\partial\rho}\right)_{T,c}\right]$$

to the right-hand side of the Navier-Stokes equation. For an isotropic fluid without macroscopic flow [so that the nonlinear hydrodynamic term $(\underline{v}\cdot\nabla)\vec{v}$ may be ignored], combination of the linearized equation of continuity and the Navier-Stokes equation leads to a small amplitude sound-wave equation,

$$\frac{\partial^2\rho}{\partial t^2} = \nabla^2 P - \frac{\rho_0}{8\pi}\,\nabla^2\left[\left(\frac{\partial\epsilon}{\partial\rho}\right)_{T,c}E^2\right] + \frac{1}{\rho_0}\left(\tfrac{4}{3}\eta+\zeta\right)\nabla^2\left(\frac{\partial\rho}{\partial t}\right). \quad (2)$$

In this equation, ρ may be expressed in terms of the independent variables P, T, c by means of the equation of state.

The acoustic-wave equation in terms of the variable P takes the form

$$\frac{1}{v_T^2}\frac{\partial^2 P}{\partial t^2} + \left(\frac{\partial\rho}{\partial c}\right)_{P,c}\frac{\partial^2 T}{\partial t^2} + \left(\frac{\partial\rho}{\partial c}\right)\frac{\partial^2 c}{\partial t^2} = \nabla^2 P + \frac{1}{\rho_0}\left(\tfrac{4}{3}\eta+\zeta\right)\left[\frac{1}{v_T^2}\nabla^2\frac{\partial P}{\partial t} + \left(\frac{\partial\rho}{\partial c}\right)_{P,T}\nabla^2\frac{\partial c}{\partial t} + \left(\frac{\partial\rho}{\partial T}\right)_{P,c}\frac{\partial T}{\partial t}\right]$$

$$-\frac{\rho_0}{8\pi}\left(\frac{\partial\epsilon}{\partial\rho}\right)_{T,c}\nabla^2 E^2 - \frac{\rho_0 E^2(\partial\epsilon/\partial\rho)^2_{c,T}}{4\pi(\epsilon+2)}\left[\frac{1}{v_T^2}\nabla^2 P + \left(\frac{\partial\rho}{\partial c}\right)_{P,T}\nabla^2 c + \left(\frac{\partial\rho}{\partial T}\right)_{P,c}\nabla^2 T\right]. \quad (3)$$

The last term, which arises from $\nabla^2(\partial\epsilon/\partial\rho)$ in Eq. (2) results in an intensity-dependent contribution to the Brillouin shift, in addition to the contribution which was pointed out by Wang.[10] The intensity-dependent effects for the gases used in this experiment are negligible and are not included in further discussion. The next to last term is the electrostrictive driving term.

The concentration diffusion equation takes the following form in the presence of an electric field:

$$\frac{\partial c}{\partial t} = D\left(\nabla^2 c + \frac{k_P}{P_0}\nabla^2 P + \frac{k_T}{T_0}\nabla^2 T\right) - \frac{D(\partial\epsilon/\partial c)\nabla^2 E}{8\pi\rho_0(\partial\mu/\partial c)_{P,T}} - \frac{DE^2\nabla^2(\partial\epsilon/\partial c)}{8\pi\rho_0(\partial\mu/\partial c)_{P,T}} \quad . \tag{4}$$

The last term produces an intensity-dependent shift of the stimulated concentration scattering analogous to the similar term in Eq. (3). The contribution of this term is also small and will not be included in further calculations.

The thermal diffusion equation in the presence of electric light fields takes the form

$$\frac{\partial T}{\partial t} + \frac{T_0}{c_P}\left(\frac{\partial s}{\partial P}\right)_{T,c}\frac{\partial P}{\partial t} - \left[\frac{k_T}{c_P}\left(\frac{\partial\mu}{\partial c}\right)_{P,T} + \frac{E^2}{8\pi\rho c_P}\left(\frac{\partial\epsilon}{\partial c}\right)_{P,T}\right]\frac{\partial c}{\partial t} = \chi\nabla^2 T - \frac{T_0}{8\pi\rho c_P}\left(\frac{\partial\epsilon}{\partial T}\right)_{P,c}\frac{\partial E^2}{\partial t} + \frac{\alpha c_0 n E^2}{8\pi\rho c_P} \quad . \tag{5}$$

The term in $E^2\,\partial c/\partial t$ in the bracket on the left-hand side is small and may be ignored. The next to last term on the right-hand side represents the coupling through thermal electrostriction. The last term represents the effect of absorption due to an optical absorption coefficient α. Since our gaseous samples are nonabsorbing, we shall put $\alpha = 0$.

We shall regard the laser field amplitude E_L as a constant parameter, and the wave (or diffusion) equations for the dynamical variables P, c, and T are then coupled to the wave equation for the scattered Stokes wave as follows:

$$\nabla^2 E_S - \frac{\epsilon_S}{c_0^2}\frac{\partial^2 E_S}{\partial t^2} = \frac{1}{c_0^2}\frac{\partial^2}{\partial t^2}E_L\left[\left(\frac{\partial\epsilon}{\partial P}\right)_{T,c}P + \left(\frac{\partial\epsilon}{\partial T}\right)_{P,c}T + \left(\frac{\partial\epsilon}{\partial c}\right)_{P,T}c\right] . \tag{6}$$

In Eqs. (3)–(5) we retain in the quadratic term E^2 only terms at the difference frequency $\omega_L - \omega_S$, i.e., only terms in $E_L E_S^*$. We thus obtain a set of four linearized coupled wave equations in the four variables c, P, T, and E_S. We may find the general dispersion relation by finding solutions in the form

$$E_S(\vec{r}, t) = \tfrac{1}{2}E_S\, e^{-ik_S z - i\omega_S t} + \text{c.c.} , \tag{7a}$$

$$P(\vec{r}, t) = \tfrac{1}{2}P_1 e^{ikz - i\omega t} + \text{c.c.} , \tag{7b}$$

$$c(\vec{r}, t) = \tfrac{1}{2}c_1 e^{ikz - i\omega t} + \text{c.c.} , \tag{7c}$$

$$T(\vec{r}, t) = \tfrac{1}{2}T_1 e^{ikz - i\omega t} + \text{c.c.} , \tag{7d}$$

with k and ω satisfying the phase and frequency matching conditions, $k = k_L + k_S$ and $\omega = \omega_L - \omega_S$.

Since the hydrodynamic modes are relatively little perturbed by the presence of the light fields, it is permissible to make the following simplification which ignores the light-intensity-dependent pulling of the hydrodynamic modes. We first solve the three by three matrix problems for the hydrodynamic modes,

$$WA = Y . \tag{8a}$$

Here A is the column vector

$$A = \begin{pmatrix} P_1^* \\ c_1^* \\ T_1^* \end{pmatrix} , \tag{8b}$$

and Y is the column vector

$$Y = \begin{bmatrix} \frac{\rho_0}{8\pi}\left(\frac{\partial\epsilon}{\partial\rho}\right)_{T,c}k^2 E_L^* E_s \\ \frac{Dk^2(\partial\epsilon/\partial c)_{P,T}}{8\pi\rho_0(\partial\mu/\partial c)_{P,T}}E_L^* E_s \\ -\frac{T_0(\partial\epsilon/\partial T)_{P,c}}{8\pi\rho_0 c_P}i\omega E_L^* E_s \end{bmatrix} . \tag{8c}$$

The matrix W has the form

$$W = \begin{bmatrix} \frac{i\omega}{v_T^2}(i\omega + bk^2) + k^2 & i\omega\left(\frac{\partial\rho}{\partial c}\right)_{P,T}(i\omega + bk^2) & i\omega\left(\frac{\partial\rho}{\partial T}\right)_{P,c}(i\omega + bk^2) \\ Dk^2\frac{k_P}{P_0} & Dk^2 + i\omega & Dk^2\frac{k_T}{T_0} \\ -i\omega\frac{T_0}{c_P}\frac{\alpha_T}{\rho_0} & -i\omega\frac{k_T}{c_P}\left(\frac{\partial\mu}{\partial c}\right)_{P,T} & i\omega + \chi k^2 \end{bmatrix} , \tag{8d}$$

where

$$b=(\tfrac{4}{3}\eta+\zeta)\rho_0^{-1}\ .$$

The solution of the matrix problem obviously gives the three complex amplitudes P_1^*, T_1^*, and c_1^* each proportional to $E_L^* E_S$. When these expressions are substituted into the wave equation for E_S, one finds an exponentially growing solution of the form

$$E_S(z,t)=\tfrac{1}{2}E_{S0}\,e^{G_{BcT}z}e^{-ik_S r-i\omega_S t}+\text{c.c.}\ ,$$

provided that the variation of the amplitude over one wavelength is small, or $G_{BcT}\ll k_S$. The gain coefficient G_{BcT} is proportional to the laser intensity, $G_{BcT}=g_{BcT}I_L$, with $I_L=|E_L|^2 c_0 n/8\pi$. The proportionality constant g_{BcT} depends on the properties of the fluid medium.

The complete solution of G_{BcT} as a function of $\omega=\omega_L-\omega_S$ is too lengthy to write out in full. It should be noted that, if the cross coupling between the acoustic-wave equation for P and the concentration equations are ignored one obtains the well-known expression for the Brillouin gain. Conversely, if the cross coupling between c and the temperature and density is ignored one would get the "pure concentration" gain. These limiting cases have been discussed previously.[2] The approximate roots of $\det(W)$ are found by considering the dimensionless parameters $(\chi k/v_s)$, (bk/v_s), and (Dk/v_s) as small. For the gas mixtures under consideration, all three of these parameters are $\simeq 0.1$. To lowest order (i.e., $\Gamma=0$), the roots of $\det(\omega)=0$ are $\omega=0,\ \pm v_s k$. In the next approximation $(0<\Gamma\ll kv_s)$ when linear terms in the small quantities are retained, the roots should correspond to the values of the frequency shift which were obtained from the decoupled-mode approximation. One obtains

$$\det(\omega)=-v_s^2(\omega-z_1)(\omega-z_2)\times(\omega-v_s k-i\Gamma)(\omega+v_s k-i\Gamma)\ . \qquad (9)$$

The two roots

$$\omega=\pm v_s k+i\Gamma k^2$$

are the propagating sound-wave modes with the damping coefficient Γ given by

$$\Gamma=\frac{k^2}{2\rho_0}\left\{(\tfrac{4}{3}\eta+\zeta)+\frac{\lambda}{c_P}(\gamma-1)+\left[Dv_s^2\Big/\rho_0\left(\frac{\partial\mu}{\partial c}\right)_{P,T}\right]\times\left[\left(\frac{\partial\rho}{\partial c}\right)_{P,T}+\frac{k_T}{c_P}\left(\frac{\partial\rho}{\partial T}\right)_{P,c}\left(\frac{\partial\mu}{\partial c}\right)_{P,T}\right]\right\}\ . \qquad (10)$$

The positive root corresponds to the Stokes-shifted stimulated Brillouin wave which has positive gain, while the negative root corresponds to the anti-Stokes wave which has negative gain.

It is important to note that in a binary mixture the sound wave has an extra damping term due to the coupling with the concentration fluctuations.[11] This extra damping depends on $(\partial\rho/\partial c)_{P,T}^2$, and consequently the sound wave is heavily damped in a mixture with a large difference of component masses. Thus the threshold of stimulated Brillouin scattering is increased by mixing. This factor is of primary importance in making possible the observation of stimulated concentration scattering. The roots which are related to the nonpropagating modes are

$$\omega_{1,2}=+ik^2\left\{\tfrac{1}{2}(\chi+\mathfrak{D})\pm\tfrac{1}{2}\left[(\chi+\mathfrak{D})^2-4\chi D\right]^{1/2}\right\}\ , \qquad (11)$$

where

$$\mathfrak{D}=D\left[1+\frac{k_T^2}{T_0 c_P}\left(\frac{\partial\mu}{\partial c}\right)_{P,T}\right]\ ,$$

when

$$k_T=0\ ,\quad \omega_{1,2}=iDk^2\ ,\quad i\chi k^2\ .$$

The root ω_1 corresponds to the concentration diffusion mode and gives stimulated concentration scattering, while the root ω_2 corresponds to the thermal diffusion mode which gives stimulated thermal Rayleigh scattering.[12] These roots have previously been obtained by Martin,[13] and by Mountain and Deutch.[14] Thus the resonances in the coupled gain expression, in the limit of small coupling between the modes, do reduce to the values predicted by the decoupled-mode approximation.

All coefficients occurring in the coupled wave equations (3)–(6) may be calculated for the gas mixtures in question. The coupling coefficients with the electric field may be expressed in terms of the polarizabilities for the individual molecular species. The Clausius-Mosotti relation and the ideal-gas law may be used to give the following relations:

$$\left(\frac{\partial\epsilon}{\partial P}\right)_{T,c}=\frac{4\pi(N_1\alpha_1+N_2\alpha_2)}{Nk_B T}\ , \qquad (12a)$$

$$\left(\frac{\partial\epsilon}{\partial c}\right)_{P,T}=\frac{4\pi\rho^2(\alpha_2-\alpha_1)}{Nm_1 m_2}\ , \qquad (12b)$$

$$\left(\frac{\partial\epsilon}{\partial T}\right)_{P,c}=\frac{-4\pi(N_1\alpha_1+N_2\alpha_2)}{T}\ ; \qquad (12c)$$

N is determined from the pressure and temperature from the virial law as discussed in Appendix A to take account of deviations from the ideal-gas law. Further corrections are not important for these quantities. The value of the polarizability α_1 for the helium atom was obtained from the calculation of Dalgano and Kingston,[15] while the values α_2 for Xe and SF_6 were obtained from the Landolt-Börnstein tables.[16]

The following coefficients are expressible in terms of thermodynamic derivatives, which are given below for the ideal-gas law. The correction terms for non-ideal-gas behavior are important,

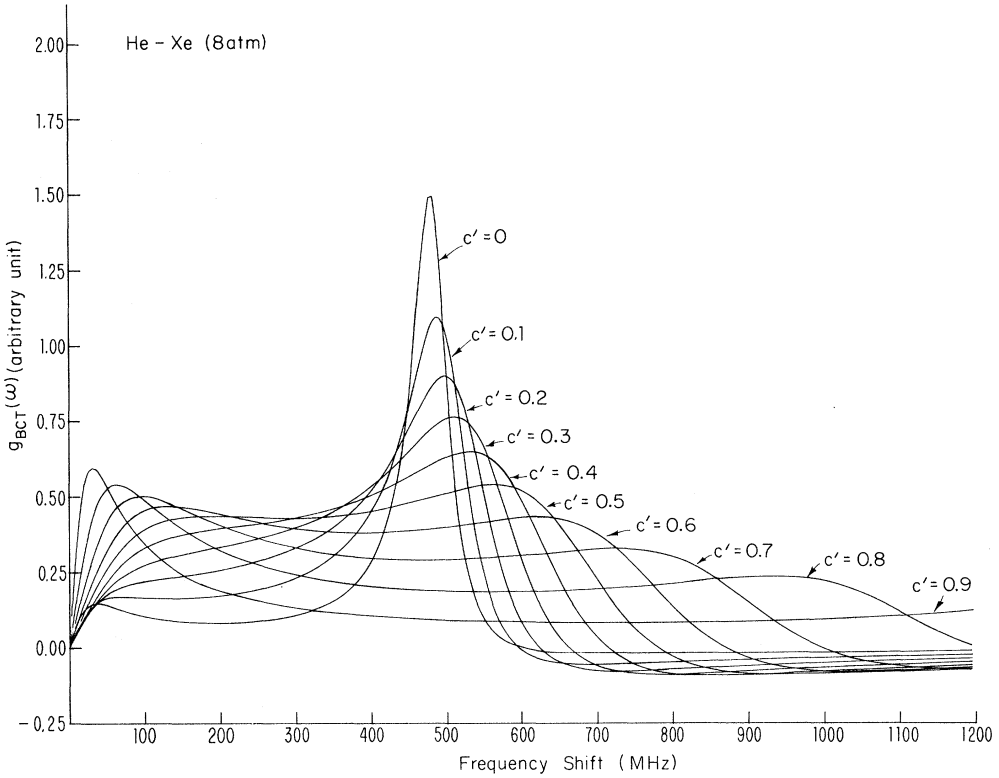

FIG. 1. The computed gain coefficient $g_{BcT}(\omega, k)$ for stimulated backward scattering of ruby laser light as a function of the Stokes frequency shift in a gaseous mixture containing 8 atm of Xe, for various partial He concentrations.

as is discussed in Appendix A.

The isothermal sound velocity v_T is given by

$$v_T^{-2} = \left(\frac{\partial \rho}{\partial P}\right)_{T,c} = \frac{\rho}{N k_B T} \quad . \tag{13}$$

Here N is the total number of molecules per unit volume, ρ is the mass density of the mixture, and k_B Boltzmann's constant. The adiabatic sound velocity v_s is given by

$$v_s^2 = \gamma v_T^2 \quad \text{with } \gamma = c_P/c_v \ . \tag{14}$$

The ratio of specific heat at constant temperature and pressure is also discussed in Appendix A. The thermal expansion coefficient is

$$\alpha_T = -\rho^{-1}\left(\frac{\partial \rho}{\partial T}\right)_{P,c} = T^{-1} \ . \tag{15}$$

The barodiffusion coefficient is given by

$$k_P = -P\left(\frac{\partial \rho}{\partial c}\right)_{P,T} \Big/ \rho^2 \left(\frac{\partial \mu}{\partial c}\right)_{P,T} \ , \tag{16}$$

with

$$\left(\frac{\partial \rho}{\partial c}\right)_{P,T} = \frac{\rho^2(m_2 - m_1)}{N m_1 m_2} \ , \tag{17}$$

$$\left(\frac{\partial \mu}{\partial c}\right)_{P,T} = \frac{k_B T \rho}{c(1-c) N m_1 m_2} \ . \tag{18}$$

The transport coefficients may be calculated by use of the Chapman-Enskog theory.[17,18] This procedure is discussed in Appendix B, where expressions are given for the viscosity η, the thermal conductivity λ, which is related to the thermal diffusivity $\chi = \lambda/\rho\, c_P$, the coefficient of diffusion D, and the thermal diffusion ratio k_T.

With the use of the expressions in the Appendices all coefficients in the matrix equations (8a)–(8d) are known, and the gain G_{BcT} may be calculated without using any adjustable parameters. The results are shown (in Fig. 1) for a gas mixture consisting of 8 atm of partial pressure of Xe to which He is added, and (in Fig. 2) for a gas mixture of 5 atm of partial pressure of SF_6 to which He is added. These results conform directly to the experimental conditions as described in Sec. IV.

The gain coefficients for the stimulated effects have, of course, a one to one correspondence to the spontaneous scattering cross section $S(k, \omega)$ which is frequency and wave-vector dependent.[19,20] This relationship is to a good approximation

$$g_{BcT}(k, \omega) \propto \omega\, S(k, \omega) \ . \tag{19}$$

The spectral density for spontaneous scattering was calculated with the same numerical values for all the coupling coefficients. Very good agreement

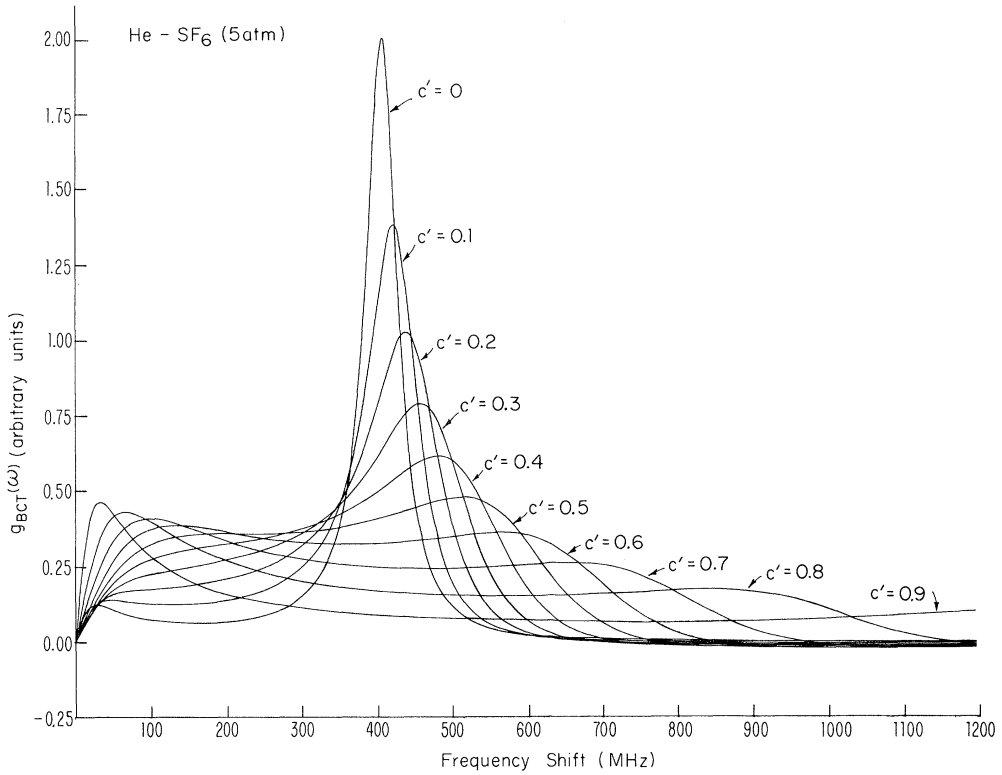

FIG. 2. The computed gain coefficient $g_{BcT}(\omega, k)$ for stimulated backward scattering of ruby laser light as a function of the Stokes frequency shift in a gaseous mixture containing 5 atm of SF_6 for various partial He concentrations.

between theory and experiment was obtained in that case.[20]

The stimulated gain coefficient shows, of course, similar features as the spontaneous process. In pure SF_6 or pure Xe a rather large and sharp resonance occurs at the Brillouin shifted frequency. As He is added, the maximum gain goes down rather rapidly. This is caused by the increased damping in the mixture of disparate masses as represented by the last term in Eq. (10). There is also an upward shift in the frequency with maximum gain, as we admix the lighter component. We also obtain an increase in gain at lower frequencies due to concentration scattering. At a relative concentration of 60% He, the gain curve as a function of frequency is very flat. Brillouin or concentration maxima can hardly be distinguished. This behavior is caused by the severe mode mixing of the concentration and acoustic overdamped waves. At still higher He concentrations the frequency shift corresponding to the maximum gain coefficient has suddenly shifted to very low values. Here stimulated concentration scattering may be said to dominate Brillouin scattering, although it must be remembered that the real situation corresponds to a mixed hydrodynamic mode. This situation is emphasized in Fig. 3, where we compare the maximum gain for the mixed mode with the gain which would be calculated on the basis of uncoupled modes. It is seen that the gain for the uncoupled electrocaloric effect g_T is always very small, and that the uncoupled concentration gain g_c would become approximately equal to Brillouin gain g_B at a relative concentration of 90% He.

In a true steady-state situation it should be expected that the frequency shift of the backward-scattered stimulated light should correspond to the maximum in g_{BcT} curve. This behavior is plotted in Fig. 4, where it is compared with the frequency shift which could be expected for Brillouin scattering from the adiabatic sound wave $k\nu_s$ and from an isothermal sound wave $k\nu_T$, as well as for pure stimulated concentration scattering Dk^2 and pure electrocaloric thermal Rayleigh scattering χk^2. It is seen that for relative He concentrations less than 60%, we have dominant Brillouin scattering, but its character changes from adiabatic to near isothermal. The light He atoms are almost completely thermalizing during the acoustic cycle, which is mostly determined by the heavy mass component. Above 60% relative He concentration an abrupt shift in the frequency should occur. The frequency difference should become very small and practically equal to Dk^2, which value would also be appropriate

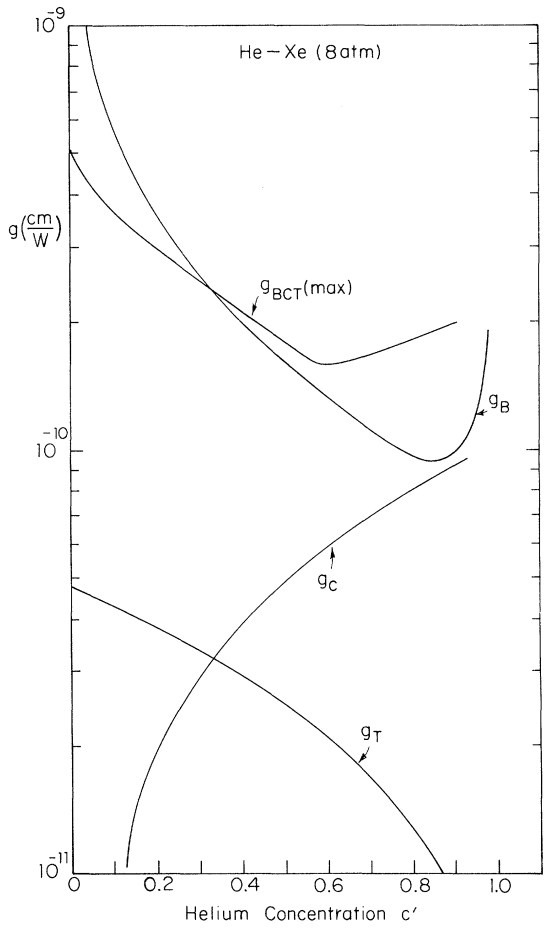

FIG. 3. The calculated gain coefficient for stimulated backward scattering, at the frequency for which it is maximum, as a function of relative He concentration in Xe-He mixtures with 8 atm of partial Xe pressure. The gain g_{BcT} is for the complete coupled mode problem, g_B is for a pure Brillouin process, g_c for a pure concentration mode, and g_T for a pure electrocaloric thermal mode.

to scattering from a pure concentration mode. The behavior for the SF_6-He mixtures is nearly identical to that of the Xe-He mixtures. We show the corresponding situation in Figs. 5 and 6 for a mixture with a partial pressure of 5 atm SF_6. These predictions of the hydrodynamic theory of binary gas mixtures will be compared with the experimental results in Sec. IV.

III. EXPERIMENTAL APPARATUS AND TECHNIQUES

The basic requirement for the stimulated-concentration-scattering experiment was to produce laser pulses with high intensity (~200 MW/cm^2) and narrow linewidth (~0.005 cm^{-1}), focus this beam into the gas mixture and analyze the spectrum of the backward-stimulated wave with a Fabry-Perot interferometer of suitably high resolution.

The required sharp frequency spectrum of the laser output was achieved by careful axial-mode selection of a relatively low-power ruby oscillator. The high intensity of the laser beam was attained by passing the beam through a ruby amplifier.

Successful completion of the experimental measurements was due to the development of an amplifier technique for generating the threshold signal needed for observation. This technique can be used to facilitate the observation of any low-gain stimulated scattering process since it reduces the required threshold power.

A. Oscillator-Amplifier

The ruby oscillator used in this experiment was a Maser Optics 868. The rod was a rectangular cut Verneuil ruby, $\frac{1}{2}$ in. diam and 6 in. long. The ruby was of very poor optical quality making single transverse-mode operation impossible. The laser cavity was 150 cm long. The rear reflector was a dielectric coated quartz flat and the front reflector was a model RR 223-4 resonant reflector from Laser Systems Corp. The resonant reflector consisted of four optically aligned quartz flats. The reflectivity of this instrument as a function of the wavelength of the incident light is a series of sharp peaks of width ~0.1 Å separated by about 1 Å. The maximum reflectivity is 64%. The reflectivity peaks were sufficiently sharp and well separated that only a single axial mode oscillated. The spectrum of the laser output was examined with a 6-cm Fabry-Perot interferometer. A typical result is shown in Fig. 7(a). It is evident that the output is single mode with a linewidth < 0.005 cm^{-1}.

The laser was Q switched by a solution of cryptocyanine dye in methanol. The dye concentration was adjusted so that the laser operated just slightly above threshold. This condition was found to produce the most reproducible output power and narrowest linewidth.

The temporal behavior of the Q-switched pulse was monitored by a TRG 105B planar photodiode (risetime < 0.3 nsec) with the output displayed on a Tektronix 519 oscilloscope. Any temporal modulation of the laser output could easily be detected. When the oscillator was carefully aligned and operated slightly above threshold, the temporal behavior of the laser pulse was as shown in Fig. 7(b). There was no visible modulation which confirmed the oscillation of only a single axial mode. If the laser was operated considerably above threshold, the time trace showed modulation due to the beating of two or more axial modes. The relatively long time duration of the laser pulse indicated by Fig. 7(b) (~50 nsec) for a laser of this type was due to the high reflectivity of the resonant reflector. As the oscillator power output was increased from ~5 to ~20 MW/cm^2 with the dye concentration also increased so that laser threshold was only

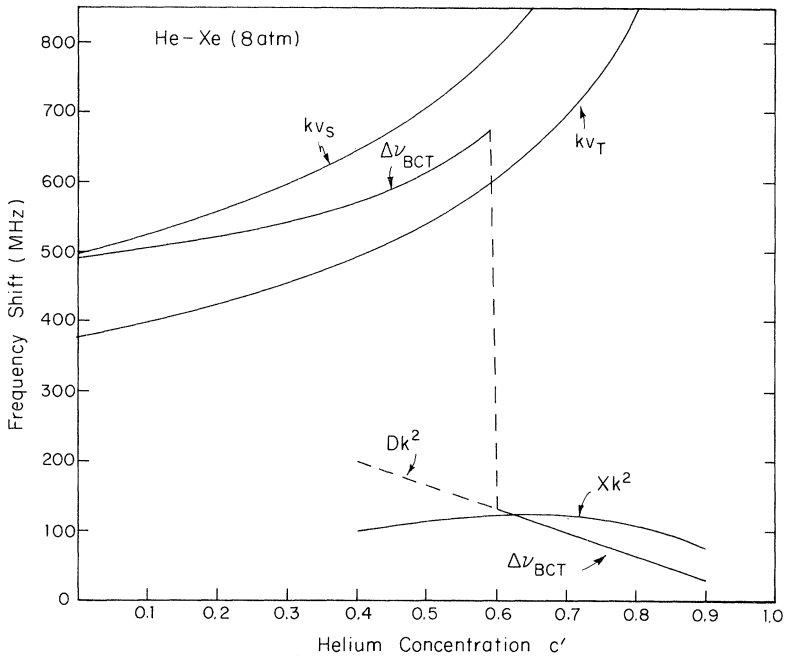

FIG. 4. Calculated curves for the frequency shift at which the gain for stimulated backward scattering in He-Xe mixtures is maximum. The following cases are shown: the coupled mode problem, the uncoupled adiabatic Brillouin scattering, the uncoupled isothermal Brillouin scattering, the pure concentration, and the pure electrocaloric scattering.

slightly exceeded, the pulse duration dropped from ~50 to ~20 nsec.

Transverse mode selection of this laser was not possible due to the poor optical quality and nonuniform pumping of the ruby rod. The beam divergence of 2 mrad was about ten times the diffraction-limited divergence indicating that approximately 100 transverse modes were oscillating.

In order to produce the high laser power required to reach threshold for stimulated concentration scattering, it was necessary to build a ruby amplifier. The advantage of the oscillator-amplifier system over a very high-power oscillator is that the high power can be reached while maintaining a simple axial mode and consequently a narrow linewidth.

The amplifier rod was a Verneuil ruby, 7 cm long and 1.5 cm diam. The maximum single pass gain for this rod was about 11.

The maximum intensity achieved with the amplifier was approximately 200 MW/cm^2. This power level however produced damage in the amplifier rod in the form of a small chip at the center of the exit face of the rod and a bubble about $\frac{1}{2}$ cm in from that surface. The reason that this rod damaged at a relatively low-power level was that it had a definite core, i.e., large optical inhomogeneity down the center of the rod, which greatly reduced the damage threshold. Also the oscillator beam had many small-diameter hot spots which gave local regions of much higher intensity than the average beam intensity. To avoid further damage to the amplifier rod, a 2:1 inverted telescope was inserted between the oscillator and the amplifier. Also a small area was ground on the beam splitter which was in front

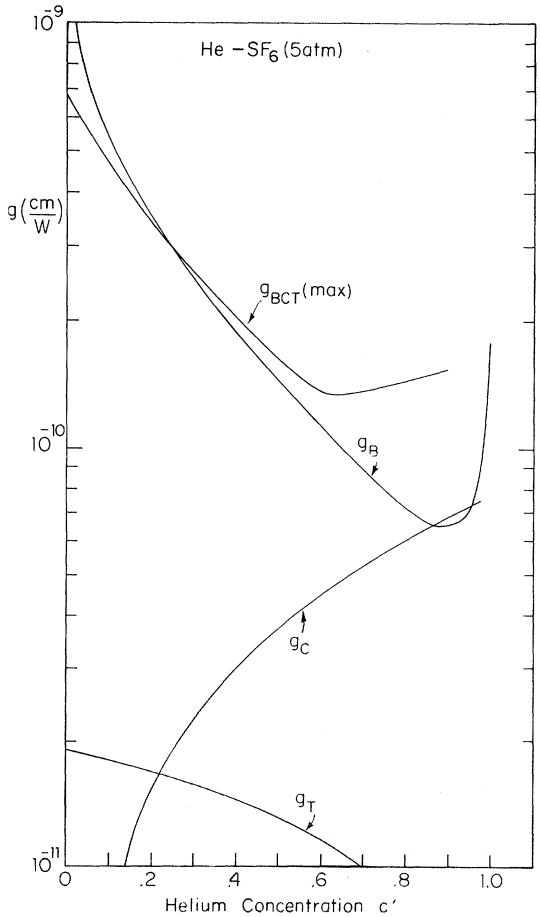

FIG. 5. Data for He-SF_6 mixtures with 5 atm of partial SF_6 pressure, corresponding to those shown in Fig. 3 for He-Xe mixtures.

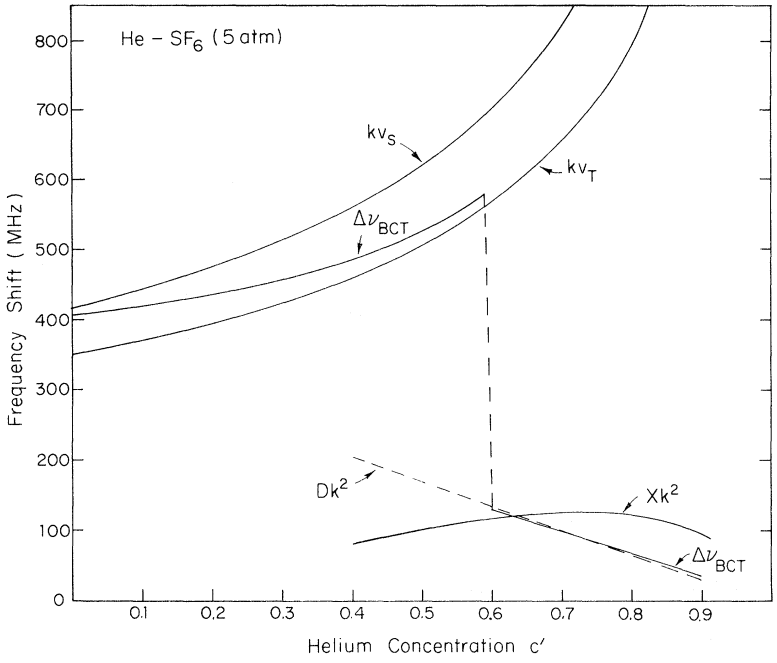

FIG. 6. Data for He-SF_6 mixtures with 5 atm of partial SF_6 pressure, corresponding to those shown in Fig. 4 for He-Xe mixtures.

of the amplifier. This ground spot scattered the center of the oscillator beam and so prevented light from traveling down the core of the amplifier rod. An aperture with diameter slightly smaller than the amplifier-rod diameter was also inserted before the amplifier. The purpose of this aperture was to prevent light from the oscillator from falling on the beveled edge of the amplifier rod and thus avoid any chance focusing of the beam in the amplifier rod. The combination of these additions was successful as no further damage to the amplifier rod occurred.

Ideally the laser should have been isolated from the cell containing the gas mixture by a Kerr cell or a Faraday rotator. Lacking this equipment, another method was used. A dye cell was placed immediately after the amplifier and a 50-nsec optical delay between the laser and the gas cell was introduced. The final arrangement for the oscillator-amplifier system is shown in Fig. 8. After passing through the amplifier and dye cell, the beam was turned by 90° by an arrangement of two prisms. The prisms also rotated the beam polarization from horizontal to vertical. The beam then traveled a distance of 6.78 m to the spherical mirror. This distance was equal to the mirror radius of curvature so the mirror reimaged the beam with 1:1 magnification at a position just to the right of the double prism as indicated in Fig. 8. The laser output was then directed into the cell containing the gas mixtures under investigation. The total time then required for light to make a round trip from the amplifier to the gas cell and back to the amplifier was about 100 nsec which is approximately the duration of the laser pulse as shown in Fig. 7(b). Thus the end of the laser pulse had left the

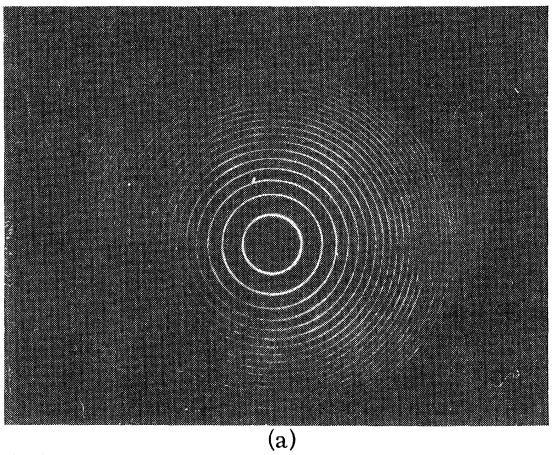

(a)

(b)

FIG. 7. (a) Frequency content of ruby laser pulse analyzed by a 6-cm Fabry-Perot etalon. (b) Oscilloscope trace of laser power output (horizontal scale: 20 nsec/div).

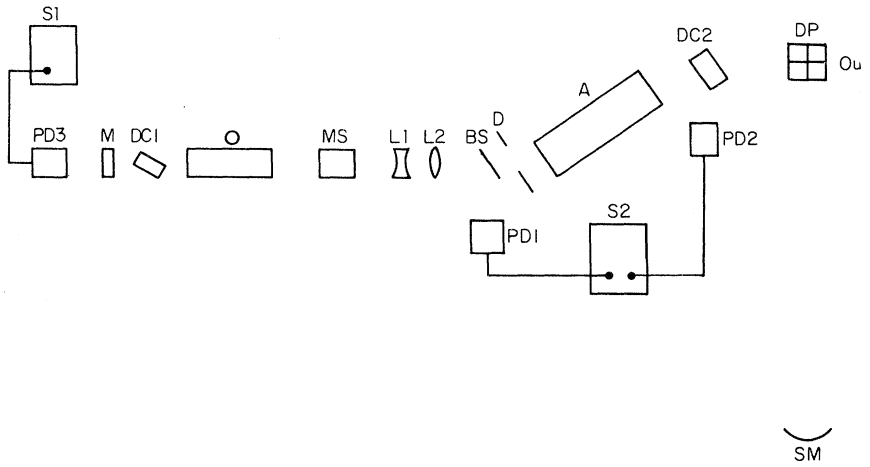

FIG. 8. Schematic diagram of oscillator-amplifier ruby laser system. A—amplifier; BS—beamsplitter; D—diaphragm; DC1—oscillator Q-switch dye cell; DC2—dye cell; L1—lens, −10-cm focal length; L2—lens, +20-cm focal length; M—oscillator rear mirror; MS—mode selector; O—oscillator; PD1—RCA 917 photodiode; PD2—ITT photodiode; PD3—TRG 105B photodiode; S1—Tektronix 519 oscilloscope; S2—Tektronic 555 oscilloscope; SM—spherical mirror, 6.78-m radius; DP—crossed polarizer quadrants.

amplifier before the front of the backscattered pulse had reached the amplifier. The dye concentration in the amplifier dye cell was adjusted so that it bleached when the laser pulse passed through but not when the backscattered pulse passed through. This introduced enough loss in the backscattered beam that it was not amplified to sufficient intensity to stimulate any further scattering.

B. Experimental Arrangement

The experimental arrangement to measure stimulated backscattering is shown in Fig. 9. The collimated linearly polarized beam from the laser entered as indicated by the arrow. The beam

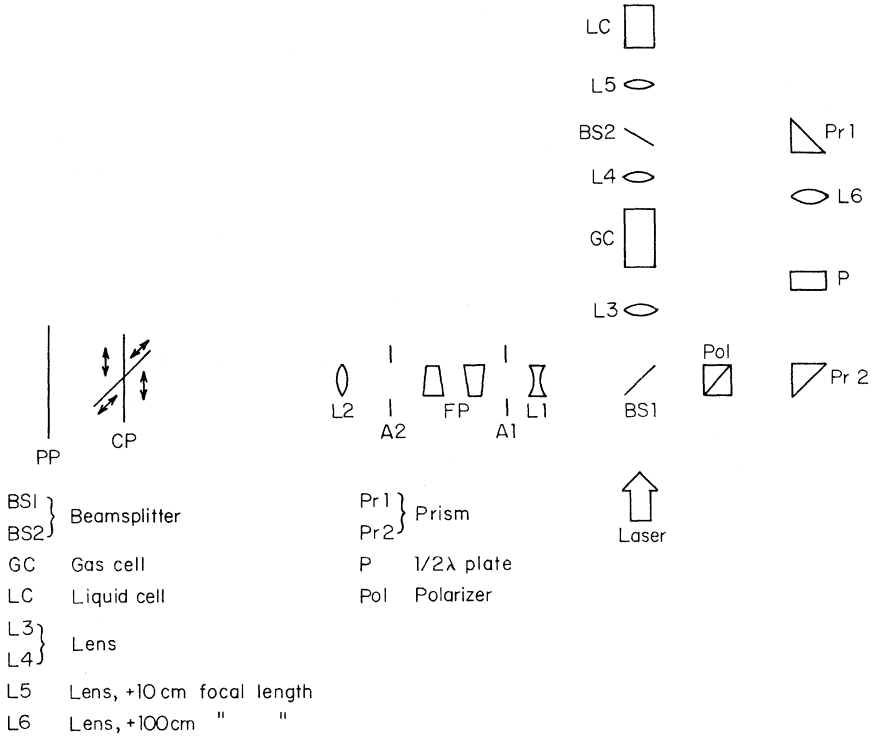

FIG. 9. Schematic diagram of experimental arrangement to measure stimulated backscattered light from gaseous mixtures: CP: crossed polarizer quadrants, PP: photographic plate, FP: Fabry-Perot, L_1 and L_2: lenses, A_1 and A_2: apertures.

passed through the glass beam splitter BS1 and was focused by lens L3 (focal length 15–40 cm) into the cell GC containing the gas mixture. After passing through the gas cell, the beam was recollimated by lens L4 (focal length 20 cm) and focused into the liquid cell LC which contained nitrobenzene. The spectrum of the light scattered in the backward direction from the nitrobenzene consisted of the stimulated Brillouin line with a frequency shift of 0.26 cm^{-1} on the Stokes side of the laser frequency, the stimulated Rayleigh wing line with a Stokes shift of 0.111 cm^{-1}, which have been investigated by Denariez and Bret, [21] and a broad diffuse wing centered at the laser frequency which is due to scattering from the thermal shear-wave mode in nitrobenzene. This spontaneous scattering has been investigated by Stegeman. [22] This diffuse-wing backscattering from the nitrobenzene served reduces the laser power required to produce observable stimulated scattering from the gas mixture in a manner which will be discussed below.

The backscattered light from the nitrobenzene was recollimated by lens L5. Approximately 8% of this beam was reflected by the glass beam splitter BS2. This portion of the beam was directed around the gas cell by the prisms Pr1, Pr2. Its polarization was rotated from vertical to horizontal by the half-wave plate P. The remainder of the backscattered light from nitrobenzene passed back into the gas cell where it interacted with the gas mixture and the laser beam in the focal volume of lens L3. Approximately 8% of the beam traveling in the backward direction out of the gas cell was reflected by the beam splitter BS1 and recombined with the portion of the light scattered from the liquid which had traveled around the gas cell.

The combined beam then passed through the Fabry-Perot interferometer (FPP). The FPP interference pattern was focused through the polarization analyzer plate CP onto the Polaroid 413 film PP. The distance between the dielectric coated quartz plates of the FPP was 6 cm. A finesse of 25 was achieved giving an instrumental resolution of 0.003 cm^{-1} (90 MHz). A typical example of the FPP interference fringes photographed with this arrangement are shown in Fig. 10. The fringes which appear in quadrants 1 and 3 are due to the light from the nitrobenzene which has traveled around the gas cell. This is then the input spectrum in the backward direction into the gas cell, consisting of the backscattered light from the nitrobenzene. Only the stimulated Brillouin line appears on the film. The Rayleigh and shear-wave wing intensity is too low to appear on the film. The wings are not sufficiently intense to expose the film, and in addition are much broader than the free spectral range of the FPP and so would appear only as a general fogging of the photograph. The FPP fringes which appear in quadrants 2 and 4 give the output spectrum from the gas cell. This consists of the nitrobenzene Brillouin wave which has simply passed through the gas cell, a portion of the incident laser beam which has been reflected from the gas-cell window, and the stimulated line from the gas mixture. By monitoring the spectrum input to the gas cell one can be certain that the line, which is attributed to the gas mixture, was not by some process coming from the nitrobenzene. The frequency shift was determined from the difference in diameter of the interference fringes which were due to the laser and stimulated backscattered light using the analysis given by Born and Wolf. [23]

The broad shear-wave wing from nitrobenzene functions in the following manner to reduce the laser power required to produce observable stimulated scattering from the gas mixture. If the nitrobenzene cells were removed and the laser simply focused into the gas mixture, the Stokes wave gain must be on the order of e^{10} in order for stimulated oscillation to occur. That is to say that the threshold for observation is $I(\omega_s) \sim I_{\text{noise}}(\omega_s) e^{20}$, where $I_{\text{noise}}(\omega_s)$ is the power of the noise field at the Stokes frequency ω_s which arises from spontaneous scattering scattering from thermal fluctuations in the material mode. Thus the threshold laser intensity I_L for an oscillator arrangement without nitrobenzene cell is determined by

$$g_{BcT} I_L z = 10 ,$$

where g_{BcT} is the Stokes-wave gain coefficient, and z is the distance over which gain occurs. Since g_{BcT} decreased with increasing He concentration c', as shown in Figs. 3 and 5, the laser intensity required to produce oscillation increased as c' increased. Without use of the nitrobenzene cell, stimulated scattering was successfully observed in gas mixtures with He concentration up to 60%. At

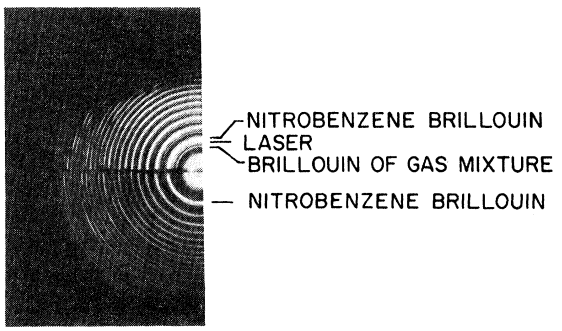

FIG. 10. Interference fringes showing spectral characteristics of light at the backward traveling input of the gas cell (lower part) and the output after stimulated backward gain (upper part). The spacing of the FP plates was 6 cm.

this point, the laser intensity required to produce oscillation was 200 MW/cm^2 and damage occurred in the amplifier rod and the higher concentrations could not be investigated.

The function of the broad shear-wave wing from nitrobenzene is to effectively increase the amplitude of $E_{\text{noise}}(\omega_s)$. When this broad spectrum light traveling in the backward direction is present in the gas mixture simultaneously with the laser wave, the gain of the medium amplifies that portion of the spectrum which is at the frequency ω_s.

This technique of amplifying a broad spectrum to produce an observable stimulated wave from a low gain process is effective as illustrated by the result that the laser intensity required to produce stimulated Brillouin scattering in SF_6 gas at 5-atm pressure dropped from 60 MW/cm^2 in the collimated beam when the beam was simply focused into the gas to 20 MW/cm^2 when this amplifier technique was used. The reduction in the laser power required to reach stimulated oscillation utilizing this technique was a crucial factor which allowed completion of the experiment with the existing laser system. It was then possible to produce stimulated scattering in gas mixtures with helium concentration as high as 90%.

It was necessary to investigate whether using the amplifier technique introduced any pulling of the frequency of the stimulated scattering in the gas mixture. This was done by studying the frequency shift of the stimulated line in gas mixtures with low helium concentrations. In these mixtures the laser intensity was great enough to produce oscillation by simply focusing into the gas mixture as well as with the amplifier technique. The shift in frequency was the same in both cases within the accuracy of the measurement.

C. Gas-Handling Equipment

A system was constructed to fill the gas call and measure the pressure of the gases contained in the cell. Before filling, the entire system was evacuated. After evacuation, the SF_6 or xenon gas was slowly leaked into the system until the desired pressure was reached. The gas mixture was made by slowly leaking helium gas into the system until the required total pressure was reached. At least 1 h was allowed for complete mixing to take place before any measurements were made. There was no observable change in the scattered light spectrum when longer mixing times were allowed.

The helium gas used in this experiment was supplied by the U. S. Navy. The xenon and SF_6 were purchased from Matheson Gas Products. The SF_6 is inexpensive and so was simply discarded whenever necessary to change concentration. However, xenon gas is quite expensive and so it was trapped in a reservoir cooled with liquid N_2 and recycled.

IV. EXPERIMENTAL RESULTS

The first experiments on stimulated concentration scattering were done in mixtures of SF_6 and He. As a preliminary to these experiments, measurements were made of the Brillouin threshold for pure SF_6 as a function of gas pressure. This was done to determine the minimum pressure of SF_6 in which stimulated Brillouin scattering could be observed and, as a byproduct, to test that the Brillouin threshold was inversely proportional to the square of the gas density as predicted by the theory. It was important to know the minimum SF_6 pressure at which the available laser power could produce stimulated scattering because, as discussed in the Introduction, the possibility of observing concentration scattering is greatest at low pressure. The results of this measurement are shown in Fig. 11. The minimum SF_6 pressure in which stimulated Brillouin scattering (SBS) was observed was 4 atm. In the range of pressure from 4 to 14 atm the experimental value of the SBS threshold power is inversely proportional to the square of the pressure, in agreement with theory.

It was decided on the basis of these results and from gain calculations, that a partial pressure of 5 atm of SF_6 would be appropriate for the investigation of stimulated scattering from He-SF_6 mixtures. The He concentration of the mixture was increased by adding He. Thus, as the He concentration increased, the total pressure also increased. The experimental results as determined by the technique described in Sec. III for the frequency shift of the stimulated backward-scattered light as a function of partial He number concentration are presented in Fig. 12. For He concentrations less than 60% the observed frequency shift is in very good agreement with the theoretical calculations. The drawn theoretical curve in Fig. 12 is taken from Fig. 6, and represents the frequency shift at which g_{BcT} is maximum. For partial pressures of helium above 8 atm, while the SF_6 partial pressure remains at 5 atm, the value of the observed frequency shift decreases rapidly toward the small values characteristic of the concentration mode. The observed shift does not show the abrupt transition, predicted by the steady-state theory, but changes relatively smoothly to small values. This discrepancy can be explained by the transient nature of the gain which becomes more pronounced as the pressure increases. The steady-state solution is only valid, if the pulse duration satisfies the condition

$$t_p \gg \Gamma_{BcT}^{-1} G_{BcT} z ,$$

where Γ_{BcT} is the frequency width of the mixed mode for which the gain is calculated. In our experimental arrangement the effective amplitude gain to reach threshold is about e^{10}. In a somewhat

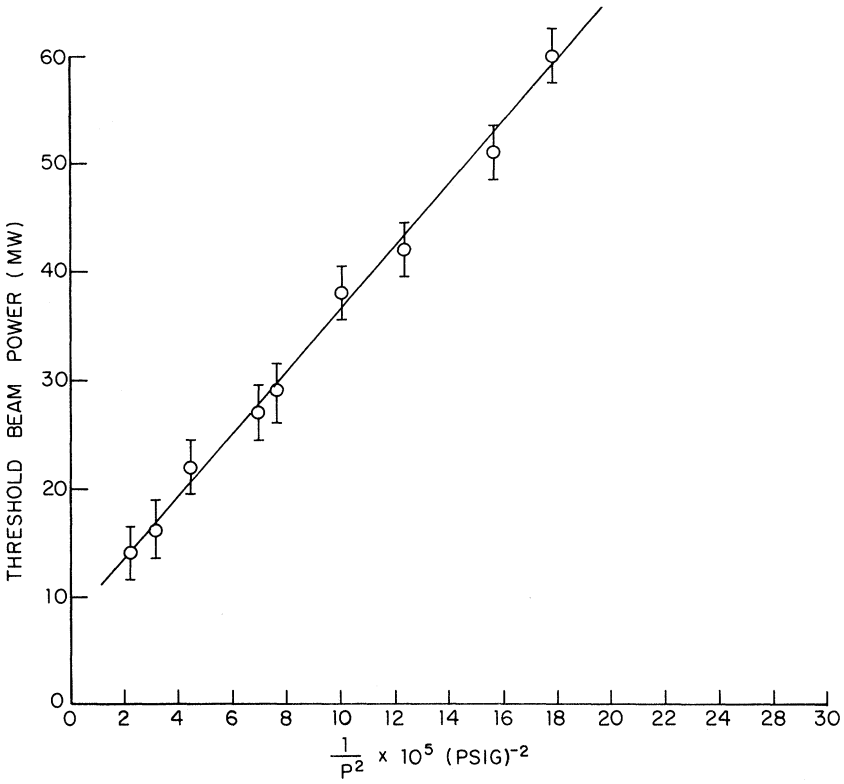

FIG. 11. The threshold pump power required for the observation of stimulated Brillouin scattering in pure SF_6 gas as a function of pressure.

transient regime the steady-state gain corresponding to the pump threshold may be as high as $G_{BcT} \simeq 40$. The width of the concentration mode Γ has the same order of magnitude as Dk^2, which decreases with increasing helium pressure. Since $t_p \sim 5\times10^{-8}$ and $(Dk^2)^{-1} \sim 2.5\times10^{-9}$ sec at 50 atm of helium, the condition for validity of the steady-state solution is clearly violated at partial helium concentrations of 90%. This is even more true, if the laser pulse has additional temporal fluctuations. At helium concentrations less than 50%, the frequency for maximum gain may be expected to be given correctly by the steady-state theory. No attempt has been made to obtain transient solutions

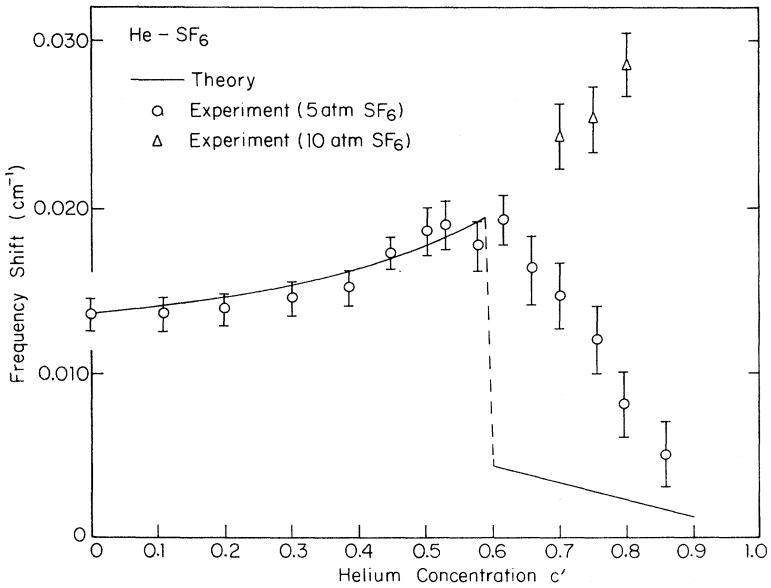

FIG. 12. The Stokes frequency shift (measured in wave-number units) of the stimulated backward scattered light in mixtures of 5 atm of SF_6, as a function of the relative He number concentration. The drawn curve is the theoretical steady-state curve, marked $\Delta\nu_{BcT}$ in Fig. 6.

for the case of the four coupled partial differential equations (3)–(6), but solutions for two coupled equations describing transient Brillouin or Raman scattering are well known.[24]

We may obtain somewhat more insight in the transient character of the solutions in our case by considering the gain curves in Fig. 2 as a function of frequency. These curves are very flat for helium concentrations between 60 and 80%. The low-frequency maximum is not pronounced. During a short laser pulse the higher-frequency components in the input signal may contribute very substantially to the over-all gain. Thus the gradual decrease in the frequency of the amplified signal is made plausible.

The threshold power necessary to observe the stimulated signal increased at first very rapidly with increasing helium concentration in agreement with the rapid increase in damping calculated for the Brillouin mode. It is difficult to make such an agreement quantitative as it requires complete knowledge of the laser field in the focus at each shot. In a qualitative manner the gain curve certainly obeyed the theoretical predictions.

It is of particular interest to note that when the same experiments were repeated with an initial SF_6 pressure of 10 atm the Brillouin mode always remained dominant. This is displayed by the triangular points in Fig. 12. This is in agreement with the theoretical calculation that at this higher pressure the Brillouin gain always remains dominant. This result may also be described in the following way. If a mixture of 5 atm of SF_6 and 20 atm of He is compressed by a factor of 2, the frequency shift of the backscattered stimulated light increases from that characteristic for concentration scattering to that characteristic for Brillouin scattering.

The range of existence for stimulated concentration scattering is therefore a narrow one indeed. It has a chance to compete effectively with stimulated Brillouin scattering only in gaseous mixtures at relatively low total pressure. Furthermore, the constituent molecules should differ as much as possible both in polarizability and in mass. Finally, the total pressure cannot be chosen too low, because then the hydrodynamic regime would not hold for the frequency shifts of interest. Furthermore, the field intensities required for threshold lie uncomfortably close to the dielectric breakdown strength for such gaseous mixtures. This difficulty was not so serious in SF_6-He mixtures. The Brillouin gain in SF_6 is somewhat higher and this molecule also attaches free electrons rather readily, so that it is used industrially as a breakdown inhibitor.

It was a problem however in Xe-He mixtures, both in the experiments of Aref'ev and Morozov[5] as well as in our first experiments with Xe. It was nevertheless considered important to demonstrate the stimulated concentration scattering also in a mixture of monatomic gases. This would remove some of the uncertainties in the calculations of transport coefficients and other properties of gases containing polyatomic molecules.

The Brillouin gain in Xe is about half the gain for SF_6 at the same pressure. Consequently a higher partial pressure of Xe was required to observe stimulated Brillouin scattering. On the basis of preliminary calculations, a Xe partial pressure of 8 atm was chosen. Even with the use of the amplifier experimental arrangement, it was observed that the electrical breakdown threshold in pure Xe at 8 atm was approximately equal to the Brillouin threshold. The breakdown threshold was measured to be $\sim 10^{11}$ W/cm^2. The actual value of this number is of little significance unless the transverse mode structure, and thus the focusing characteristics of the beam, are specified. However, this observed threshold is in agreement with the results of an earlier study of optically induced gas breakdown in the noble gases.[25]

In order to make accurate measurements, it was necessary to avoid gas breakdown since the breakdown may cause thermal Brillouin or Rayleigh scattering to occur[6] which confused earlier observations. It was discovered that by focusing the laser into the gas mixture with a lens of 40-cm focal length, instead of 20 cm, the gas breakdown did not occur in our amplifier-cell arrangement.

The experimental results for the observed frequency shift of the stimulated backscattered light are very similar as those for SF_6-He mixtures. This is not surprising, since the theoretical results also showed a striking similarity. Experimental data for the He-Xe mixtures are compared with the theory of the Stokes shift for maximum g_{BcT} in Fig. 13. The same gradual transition of the shift toward smaller values characteristic of stimulated concentration scattering is observed for partial helium concentration above 60%. The same discussions about the transient nature of the gain characteristics applies here.

V. DISCUSSION AND CONCLUSION

The results provide a striking confirmation of the validity of the hydrodynamic equations for binary gas mixtures in the frequency range between 10^8 and 10^{10} Hz. Stimulated concentration scattering is shown to be a relatively rare phenomenon, observable only in a very restricted range of parameters. The binary gas mixture must contain two components of very large differences in mass and polarizability, while the total pressure must be high enough so that the mean free path is smaller than the scattering length, while the pressure must be low enough so that the stimulated Brillouin scatter-

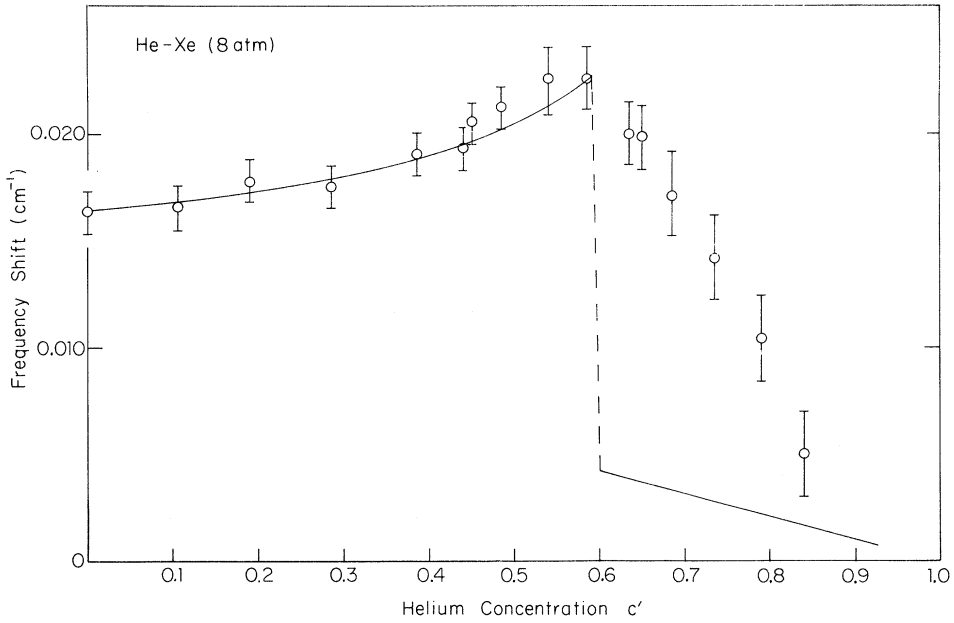

FIG. 13. The Stokes frequency shift (measured in wave-number units) of the stimulated backward scattered light in mixtures of 8 atm of Xe, as a function of the relative He number concentration. The drawn curve is the theoretical steady-state curve, marked $\Delta\nu_{BcT}$ in Fig. 4.

ing does not dominate at all concentrations. It may be safely concluded that stimulated concentration scattering may be ignored in considering problems of propagation of high-power laser beams through the atmosphere and most other fluid media. The effect should be observable in mixtures such as He-CF_4 or He-C_2F_6, and perhaps in He-Ar.

It is very important to avoid dielectric breakdown and plasma formation for obtaining quantitative agreement between theory and experiment. The experimental technique of using an input signal from an auxiliary scattering cell substantially reduces the pump power threshold. This technique should be generally useful in observing stimulated processes with low gain. It is believed that our experiments constitute the first unambiguous demonstration of stimulated concentration scattering. The earlier experiments, mentioned in the Introduction, on stimulated concentration scattering may be critically reanalyzed in terms of the theory. The first experiment[1] was performed in a liquid mixture of n-hexane (58% weight concentration) and nitrobenzene (42%). However, the ratio of the gain constants in the decoupled-mode approximation is $g_c/g_B \simeq 1.25\times10^{-5}$ which throws considerable doubt on the interpretation of this experiment. Near the critical point in a binary mixture where $\partial\mu/\partial c \to 0$, the concentration gain could become large. However, the diffusion constant D approaches zero at the same time. Thus the correlation time for concentration fluctuations becomes large $\sim 10^{-3}$ sec. The steady-state analysis breaks down for solid-state laser pulses, and even with gas laser beams it would be difficult to maintain the required coherence for such long times. A transient analysis must be made and the experimental difficulties would be further enhanced by the large spontaneous critical opalescence and large losses per unit length of the pump. Amplification of this spontaneous emission at high intensities may, however, be detectable.

The second experiment[5] was done with a Xe and He mixture with He concentration $c' = 0.9$. This is clearly a good choice. At this concentration, the Brillouin shift should be 0.0479 cm^{-1} rather than 0.055 cm^{-1} as reported. The gain ratio should be $g_c/g_B = 21$ in contrast to the estimate of $g_c/g_B = 0.1$ as estimated in the reference. The observed concentration shift 0.033–0.042 cm^{-1} agrees with the value $\Delta\nu_c = Dk^2/2\pi c = 0.032$ cm^{-1}. At a higher total pressure, the stimulated Brillouin scattering should dominate the concentration scattering as correctly stated. This should however not occur at a total pressure as low as 4 atm. Also at the low pressures used in the experiment the condition for the validity of the hydrodynamic equations is not satisfied. Since positive effects were only observed in the presence of gas breakdown this experiment must be considered inconclusive. Sparks lead to low-frequency scattering even in pure noble gases, presumably caused by thermal Rayleigh scattering.

Stimulated concentration scattering is a rare phenomenon. The amount of information it provides about fluid mechanics and structure of fluid mixtures is very limited compared to that provided by spontaneous concentration scattering. The combination of the spontaneous and stimulated scattering data in the He-SF_6 and He-Xe mixtures reaffirms the confidence in the correctness of the hydrodynamic equations in describing the behavior of fluid

mixtures under extreme conditions of disparate mass and very high frequencies.

ACKNOWLEDGMENTS

The authors are indebted to Dr. C. S. Wang for numerous helpful discussions and advice about the numerical calculations. The assistance of Dr. M. Matsuoka during the early phase of the work and discussions with Dr. W. S. Gornall during the later stage are also gratefully acknowledged.

APPENDIX A: NON-IDEAL-GAS CORRECTIONS

The well-known equation of state for the ideal gas

$$P = Nk_BT ,$$

needs some correction even at atmospheric pressure. The virial equation of state describes these corrections as a power series expansion in the number density

$$\frac{P}{Nk_BT} = 1 + B(T)\left(\frac{N}{N_a}\right) + C(T)\left(\frac{N}{N_a}\right)^2 + \cdots , \quad \text{(A1)}$$

where N_a is Avogadro's number and $B(T)$, $C(T)$ are the second and third virial coefficients.

From the statistical mechanical expressions for the virial coefficients, it becomes evident that the second and third coefficients represent deviations from ideal behavior when collisions between two and three molecules become important. As the pressure increases, more virial coefficients must be included. As an indication of the contribution of the second and third virial coefficients for the gases of interest, the following results are found at 0 °C:

SF_6 at 10 atm, $\frac{P}{Nk_BT} = 1 - 0.12 + 0.005$;

Xe at 10 atm, $\frac{P}{Nk_BT} = 1 - 0.06 + 0.0008$;

He at 100 atm, $\frac{P}{Nk_BT} = 1 + 0.05 + 0.002$.

The third virial coefficients are not significant in this work and this is consistent with the calculations of the transport coefficients of Appendix B, where only binary collisions are considered. It is perhaps interesting to note that the sign of the second-virial-coefficient correction is different for the heavy gases and for helium. This result is due to the fact that the interaction between the heavy molecules is dominated by the strong attractive part of the potential. The attractive potential for the helium atoms is weak, and thus the atomic interactions are dominated by the excluded volume effect due to the short-range repulsive part of the potential. In mixtures with a 10:1 ratio of helium to heavy-gas number density, at pressures low enough that the third virial coefficients do not contribute significantly, the ideal-gas law is not a bad approximation.

For the gas mixture, the second virial coefficient is given by[18]

$$B(T)_{\text{mixture}} = (1-c')^2 B_1(T) + c'^2 B_2(T) + 2c'(1-c')B_{12} , \quad \text{(A2)}$$

where B_1, B_2 are the virial coefficients calculated from the potential functions for molecules of type 1 and 2, and B_{12} is calculated from the potential function which characterizes the interaction between the two molecules.

The virial coefficients are calculated from the intermolecular potential $\phi(r)$ where r is the molecular separation. The second virial coefficient is given by

$$B(T) = -2\pi N_a \int_0^\infty [e^{-\phi(r)/kT} - 1] r^2 dr .$$

Hirschfelder, Curtiss, and Bird[18] have given numerical values for the reduced second virial coefficients B^*:

$$B^* = \frac{B}{b_0} \quad \text{and} \quad B_k^* = T^{*k}\left(\frac{d^k B^*}{dT^{*k}}\right) ,$$

with

$$b_0 = \tfrac{2}{3}\pi N_a \sigma^3 \text{ (second virial coefficient for hard-sphere molecules)}$$

for the case of the Lennard-Jones (6-12) potential,

$$\phi(r) = 4\epsilon[(\sigma/r)^{12} - (\sigma/r)^6] .$$

The relevant values for the gain calculations are given in Table I.

The non-ideal-gas corrections are included in the calculations by observing that there are a set of gas parameters which are more or less fundamental. These parameters are fundamental in the sense that all of the other gas parameters, thermodynamic derivatives, and transport coefficients depend upon the values of these fundamental parameters. Thus if these fundamental parameters are corrected for the nonideal behavior of the gas mixtures, the corrections to all the remaining parameters and transport coefficients will be made automatically.

These fundamental parameters are the pressure (or number density), isothermal coefficient of expansion α_T, specific heats at constant volume and at constant pressure, and the isothermal sound velocity. The non-ideal-gas corrections for these parameters can be derived from the virial expansion equation (A1) using the thermodynamic expressions for the various parameters. The derivation is straightforward and will be omitted, and the results for the gas mixture are given as follows:

$$P_1 = N_1 k_B T\left[1 + \frac{B_1}{\tilde{v}}\right] , \quad N_1 = \frac{P_1}{k_B T}\left(1 - \frac{B_1}{\tilde{v}}\right) ,$$

TABLE I. Second virial coefficient and its derivatives for the pure gases and mixtures.

	T^*	b_0	$B^*(T^*)$[a]	$B_1^*(T^*)$[a]	$B_2^*(T^*)$[a]
Helium	28.767	21.56	0.52673	−0.01180	−0.08414
SF_6	1.4634	211.0	−1.2622	2.5009	−6.0434
Xenon	1.2838	81.04	−1.6229	3.0213	−7.4610
SF_6-He	6.4883	83.36	0.34887	0.35756	−0.84055
Xe-He	6.0772	45.97	0.3270	0.3781	−0.9069

[a]These values from Ref. 18.

$$P = Nk_BT\left[1 + \frac{B_{\text{mix}}}{\tilde{v}}\right], \quad N = \frac{P}{k_BT}\left(1 - \frac{B_{\text{mix}}}{\tilde{v}}\right),$$

$$\alpha_T = \frac{1}{\tilde{v}}\left(\frac{\partial \tilde{v}}{\partial T}\right)_P = \frac{1}{T}\left(1 + \frac{B_{\text{mix}}/\tilde{v}}{1 + B_{\text{mix}}/\tilde{v}}\right),$$

$$c_v = c_v^0 - \left(\frac{2B_{\text{mix}}}{\tilde{v}}\right) + \frac{B_{2\text{mix}}}{\tilde{v}}\frac{Nk}{\rho},$$

$$c_P = c_P^0 - \frac{B_{2\text{mix}}}{\tilde{v}}\frac{Nk}{\rho},$$

$$v_T^2 = \frac{Nk_BT}{\rho}\left(1 + \frac{2B_{\text{mix}}}{\tilde{v}}\right),$$

where $\tilde{v} = N_a/N$, P_1 is the partial pressure of the heavy gas, and c_v^0 and c_P^0 are the ideal-gas values of specific heat. Since the value of N appears in $\tilde{v}$, the expressions for the number density must be evaluated in an iterative fashion.

It is a well-known result from kinetic theory that the heat capacity at constant volume c_v for a monatomic ideal gas is $\frac{3}{2}Nk_B/\rho$, which is due to the contribution of $\frac{1}{2}Nk_B/\rho$ from each of the three translational degrees of freedom. For a polyatomic molecule the specific heat depends on the frequency at which the measurement is made. For frequencies less than $1/\tau_R$, where τ_R is the rotational relaxation time (the time which is required for a molecule to change its rotational energy) the three rotational degrees of freedom will each contribute $\frac{1}{2}Nk_B/\rho$ to the specific heat. Similarly, for frequencies less than $1/\tau_v$, where τ_v is the vibrational relaxation time, the vibrational modes (15 for SF_6) can each take up energy and thus contribute to the specific heat.

The time between collisions τ_c can be calculated from kinetic energy considerations with a knowledge of the gas viscosity η:

$$\tau_c = \eta \times 10^{-5} \text{ sec}/12.66\,P(\text{atm}).$$

For SF_6 at 5 atm, $\tau_c \simeq 10^{11}$ sec. A value for the rotational relaxation time $\tau_R = 2.5\,\tau_c$ estimated from the theory of Sather and Dahler[26] has given good agreement with measurements of sound attenuation in SF_6 by Holmes and Stott.[27] Thus for frequencies less than 5000 MHz the rotational degrees of freedom contribute to the specific heat.

O'Connor[28] and Holmes and Stott[27] have shown however that the vibrational relaxation time $\tau_v \sim 10^3\tau_c$ and the experimental results show that for frequencies above 30 MHz the vibrational degrees of freedom do not contribute to the specific heat.

The frequencies of the material excitation in our experiment are ~100–500 MHz, as shown in Sec. IV. In this region the specific heat at constant volume for the SF_6 is $3\,Nk_B/\rho$ from the 3 translational and 3 rotational degrees of freedom. The specific heats for the He-SF_6 mixture are

$$c_{v\,\text{mix}} = (3N_{SF_6} + \tfrac{3}{2}N_{He})k_B/\rho,$$

$$c_{P\,\text{mix}} = c_{v\,\text{mix}} + Nk_B/\rho.$$

For the monatomic xenon gas of course these considerations do not apply and $c_v = \frac{3}{2}Nk_B/\rho$.

The bulk viscosity ζ of the polyatomic molecule is also related to the transfer of energy to internal degrees of freedom. The bulk viscosity is related to relaxation times by[18]

$$\zeta = (Nk_B^2T/c_v^2)\sum_l c_v^{(l)}\tau_l,$$

where $c_v^{(l)}$ is the contribution of the particular degree of freedom to the specific heat per molecule c_v. For SF_6 at 5-atm pressure $\zeta = 0.34\,\eta$. For xenon, the bulk viscosity is zero since there are no internal degrees of freedom.

One might reasonably be concerned that the addition of helium to the SF_6 would substantially decrease the relaxation times and allow vibrational contributions to enter the specific heats, thermal conductivity, and bulk viscosity. However the recent investigation of spontaneous scattering from the He-SF_6 mixtures made by Gornall[19] *et al.* indicate that the vibrational degrees of freedom are in fact, not excited.

APPENDIX B: CALCULATION OF GAS-TRANSPORT COEFFICIENTS

The transport coefficients may be expressed in terms of Chapman-Cowling integrals which are defined to describe a binary collision between molecules of type i and j,

$$\Omega_{ij}^{(l,s)} = \left(\frac{2\pi k_BT}{\mu_{ij}}\right)^{1/2}\int_0^\infty\int_0^\infty e^{-\gamma_{ij}^2}\gamma_{ij}^{2s+3} \times (1 - \cos l\theta)\,b\,db\,d\gamma_{ij}.$$

In these integrals, μ_{ij} is the reduced mass of the colliding molecules i and j, θ is the angle by which the molecules are deflected in the center-of-gravity coordinate system, b is the impact parameter, and γ_{ij} is the reduced initial relative speed of the colliding molecules given by

$$\gamma_{ij} = \left(\frac{\mu_{ij}}{2k_BT}\right)^{1/2} g_{ij},$$

where g_{ij} is the initial relative velocity of the two

molecules. The most satisfactory calculations of $\Omega_{ij}^{(l,s)}$ are those made on the basis of the Lennard-Jones (6-12) potential given in Appendix A, which describes reasonably well the interaction between spherical nonpolar molecules.

The Chapman-Enskog theory considers only binary collisions so the results are not applicable at densities sufficiently high that three-body collisions become important. The theory also assumes that the molecular mean free path is small compared to the dimensions of the container, so that surface effects are not important. The Chapman-Enskog theory is therefore most useful for describing the properties of a dense gas.

Strictly speaking, the Chapman-Enskog theory applies only to monatomic gases. Since inelastic collisions occur between molecules with internal degrees of freedom, the kinetic energy is not conserved upon collision, although clearly mass and momentum are conserved. Consequently, the viscosity and diffusion are not appreciably affected by the presence of internal degrees of freedom, and the theory of monatomic gases may be applied to polyatomic molecules with success, provided the molecules are approximately spherical. However, the thermal conductivity is significantly affected by internal degrees of freedom. For a monatomic gas, the thermal conductivity is related to the viscosity by

$$\lambda = \frac{15}{4}\frac{R}{M}\eta ,$$

where M is the molecular weight of the gas, and R is the gas constant. This relation has been confirmed experimentally.

The specific heat and bulk viscosity of the gas are also affected by the transfer of energy to internal degrees of freedom of the molecules. The magnitude of contribution of the internal degrees of freedom depends of course on the frequency at which the measurement is made. This point was discussed in Appendix A in connection with the calculation of the specific heat. The contribution of the internal degrees of freedom to the thermal conductivity can then be given by a correction term which depends upon the specific heat:

$$\lambda = \frac{15}{4}\frac{R}{M}\eta\left(\frac{4}{15}\frac{\tilde{c}_v}{R}+\frac{3}{5}\right) . \qquad \text{(B1)}$$

This formula was first proposed by Eucken and gives good agreement with experimental results. For a monatomic gas $\tilde{c}_v = \frac{3}{2}R$, and the Eucken formula reduces to the thermal conductivity for monatomic gas.

The calculation of the transport coefficients is quite involved and has been described by Chapman and Cowling[17] and also by Hirschfelder, Curtiss, and Bird.[18] All of the results presented here are those which arise from the first-order approximation of the Chapman-Enskog solution of the Boltzmann equation. The values of the Chapman-Cowling integrals (CCI) which are used are those calculated for the Lennard-Jones (6-12) potential. The values of the potential parameter ϵ and collision diameter σ are given in Table II. For a gas mixture, the collision diameter is given by

$$\sigma_{12} = \tfrac{1}{2}(\sigma_1+\sigma_2) ,$$

and the potential parameter is

$$\epsilon_{12} = (\epsilon_1\epsilon_2)^{1/2} .$$

The CCI are calculated as functions of the reduced temperature $T^* = Tk_B/\epsilon$, where k_B is the Boltzmann constant. The transport coefficients are given in terms of reduced integrals $\Omega^* = \Omega/\Omega_{\text{rigid sphere}}$. The values of T^* and the CCI of interest $[\Omega_{(11)}^{(2,2)*}(T_1^*)$, $\Omega_{(22)}^{(2,2)*}(T_2^*)$, $\Omega_{12}^{(2,2)*}(T_{12}^*)$, $\Omega_{12}^{(1,1)*}(T_{12}^*)]$ are also given. Certain ratios of the CCI appear frequently. They are

$$A^* = \Omega^{(2,2)*}/\Omega^{(1,1)*} ,$$

$$B^* = (5\Omega^{(1,2)*} - 4\Omega^{(1,3)*})/\Omega^{(1,1)*} ,$$

$$C^* = \Omega^{(1,2)*}/\Omega^{(1,1)*} .$$

These values are also given in Table II. For calculations pertaining to the mixtures, it is convenient to introduce a parameter M_{12} given by

$$M_{12} = 2M_1M_2/(M_1+M_2) ,$$

where M_1, M_2 are the molecular weights of the component species.

1. *Viscosity*

To a first approximation, the viscosity of a pure gas is given by

$$\eta_i = 2.6693\times10^{-5}\frac{(M_iT)^{1/2}}{\sigma_i^2\Omega_i^{(2,2)*}}\ \frac{\text{g}}{\text{cm sec}} . \qquad \text{(B2)}$$

This result may be used to obtain the viscosities of both pure gases η_1, η_2. To obtain viscosity of the mixture, it is convenient to introduce a viscosity η_{12} which is given by Eq. (B2) with i replaced by 12. The viscosity of a binary mixture is then given by

$$\frac{1}{\eta_{\text{mix}}} = X_\eta\left(\frac{1+Y_\eta/X_\eta}{1+Z_\eta}\right) , \qquad \text{(B3)}$$

where

$$X_\eta = \frac{(1-c')^2}{\eta_1}+\frac{2c'(1-c')}{\eta_{12}}+\frac{c'^2}{\eta_2} ,$$

$$Y_\eta = \tfrac{3}{5}A_{12}^*\left[\frac{(1-c')^2}{\eta_1}\left(\frac{M_1}{M_2}\right)+\frac{2(1-c')c'}{\eta_{12}}\times\left(\frac{(M_1+M_2)^2}{4M_1M_2}\right)\left(\frac{\eta_{12}^2}{\eta_1\eta_2}\right)+\frac{c_1'^2}{\eta_2}\ \frac{M_2}{M_1}\right] ,$$

TABLE II. Transport coefficients and other characteristic parameters for the pure gases He, SF_6, Xe.

	σ[a] (Å)	ϵ/k_B[a] (°K)	M (g)	T[b]	$\Omega^{22}_{(i,i)}(T^*)$[a,b]	$10^{24}\alpha$ (cm^3)	$10^4\eta$ (g/cm sec)	$10^{-3}\lambda$ (erg/gm sec °K)	$10^4 l$ (cm) (P in atm)	y		
Helium	2.576	10.22	4.003	28.767	0.706	0.2051	1.955	15.24	$\frac{0.1770}{P}$	$0.3520P$		
SF_6	5.51	200.9	146.07	1.463	1.328	4.537	1.549[b]	0.4102	$\frac{0.0209}{P}$	$2.978P$		
Xe	4.055	229	131.1	1.284	1.407	4.146	2.267	0.5382	$\frac{0.0346}{P}$	$1.800P$		
	σ_{12}[a] (Å)	ϵ_{12}/k_B[a] (°K)	M_{12} (g)	T_{12}[b]	$\Omega^{22}_{12}(T^*)$[a,b]	$\Omega^{11}_{12}(T^*)$[a,b]	$\eta_{12}\times 10^4$ (g/cm sec)	$10^{-3}\lambda_{12}$	D (cm^2/sec)	A_{12}[b,a]	B_{12}[b,a]	C[b,a]
SF_6–He	4.043	45.31	3.896	6.488	0.885	0.8013	0.8832	3.536	$\frac{0.3623}{P}$	1.104	1.091	0.9387
Xe–He	3.3155	48.38	3.884	6.077	0.894	0.8106	1.297	5.207	$\frac{0.5316}{P}$	1.103	1.096	0.9377

[a]Experimental value.

[b]These values from Ref. 2.

$$Z_\eta = \tfrac{3}{5}A^*_{12}\left\{(1-c')^2\left(\frac{M_1}{M_2}\right) + 2c'(1-c') \times \left[\frac{(M_1+M_2)^2}{4M_1M_2}\left(\frac{\eta_{12}}{\eta_1}+\frac{\eta_{12}}{\eta_2}\right)-1\right] + c'^2\left(\frac{M_2}{M_1}\right)\right\} .$$

2. *Thermal Conductivity*

For a pure gas the thermal conductivity is given by

$$\lambda_i = 8292.5\,\frac{(T/M_i)^{1/2}}{\sigma_i^2\,\Omega_i^{(2,2)*}}\ \frac{\text{erg}}{\text{cm sec °K}} \quad . \tag{B4}$$

For the polyatomic SF_6 molecules, $\tilde{c}_v = 3R$ so this result must be multiplied by $\frac{7}{5}$ (Eucken correction). The parameter λ_{12} is again given by the expression for λ_i with $i=12$. The thermal conductivity for a gas mixture is given by

$$\frac{1}{\lambda_{\text{mix}}} = X_\lambda\left(\frac{1+Y_\lambda/X_\lambda}{1+Z_\lambda}\right) , \tag{B5}$$

where

$$X_\lambda = \frac{(1-c')^2}{\lambda_1} + \frac{2c'(1-c')}{\lambda_{12}} + \frac{c'^2}{\lambda_2} ,$$

$$Y_\lambda = \frac{(1-c')^2}{\lambda_1}\,U^{(1)} + \frac{2c'(1-c')}{\lambda_{12}}\,U^{(Y)} + \frac{c'^2}{\lambda_2}\,U^{(2)} ,$$

$$Z_\lambda = (1-c')^2U^{(1)} + 2c'(1-c')U^{(Z)} + c'^2U^{(2)} ,$$

$$U^{(1)} = \tfrac{4}{15}A^*_{12} - \tfrac{1}{2}\left(\tfrac{12}{5}B^*_{12}+1\right)\frac{M_1}{M_2} + \frac{1}{2}\,\frac{(M_1-M_2)^2}{M_1M_2} ,$$

$$U^{(2)} = \tfrac{4}{15}A^*_{12} - \tfrac{1}{12}\left(\tfrac{12}{5}B^*_{12}+1\right)\frac{M_2}{M_1} + \frac{1}{2}\,\frac{(M_2-M_1)^2}{M_1M_2} ,$$

$$U^{(Y)} = \tfrac{4}{15}A^*_{12}\left(\frac{(M_1+M_2)^2}{4M_1M_2}\right)\frac{\lambda^2_{12}}{\lambda_1\lambda_2} - \tfrac{1}{12}\left(\tfrac{12}{5}B^*_{12}+1\right) - \frac{5}{32A^*_{12}}\left(\tfrac{12}{5}B^*_{12}-5\right)\frac{(M_1-M_2)^2}{M_1M_2} ,$$

$$U^{(Z)} = \tfrac{4}{15}A^*_{12}\left[\frac{(M_1+M_2)^2}{4M_1M_2}\left(\frac{\lambda_{12}}{\lambda_1}+\frac{\lambda_{12}}{\lambda_1}\right)-1\right] - \tfrac{1}{12}\left(\tfrac{12}{5}B^*_{12}+1\right) .$$

3. *Coefficient of Diffusion*

The coefficient of diffusion for a binary mixture is given by

$$D = \frac{2.628\times 10^{-3}\,(T^3/M_{12})^{1/2}}{P\sigma^2_{12}\,\Omega^{(1,1)*}_{12}(T^*_{12})}\ \frac{\text{cm}^2}{\text{sec}} , \tag{B6}$$

where P is the pressure in atmospheres.

4. *Thermal-Diffusion Ratio*

The thermal-diffusion ratio for a binary gas mixture is given in first approximation to be

$$k_T = \frac{c'(1-c')}{6\lambda_{12}}\,\frac{s^{(1)}(1-c') - s^{(2)}c'}{X_\lambda + Y_\lambda}\,(6c^*_{12}-5) , \tag{B7}$$

TABLE III. Transport coefficients for the He-SF_6 (5 atm) mixture.

He c'	He P lb/in.^{2}	$10^2\rho$ (g/cm^3)	$10^4\eta$ (g/cm sec)	$10^{-2}\lambda$ (erg/g sec °K)	$10^2 D$ (cm^2/sec)	$10^{-6} c_P$ (erg/g °K)	γ	$10^{-4} v_T$ (cm/sec)	Γ (MHz)
0	0	3.27	1.55	4.10	6.71	2.44	1.41	1.21	26.1
0.1	9	3.28	1.58	6.70	5.99	2.59	1.42	1.29	47.0
0.2	20	3.29	1.61	9.84	5.29	2.78	1.44	1.38	68.6
0.3	34	3.31	1.65	13.7	4.59	3.02	1.45	1.48	91.2
0.4	53	3.33	1.69	18.6	3.91	3.34	1.47	1.60	114
0.5	80	3.36	1.74	24.8	3.23	3.78	1.50	1.76	138
0.6	121	3.40	1.80	33.3	2.57	4.42	1.52	1.98	162
0.7	189	3.48	1.88	45.2	1.91	5.45	1.55	2.28	183
0.8	325	3.63	1.96	63.1	1.26	7.40	1.59	2.76	199
0.9	741	4.08	2.04	93.2	0.622	12.4	1.63	3.76	186

where

$$s^{(1)} = \frac{M_1+M_2}{2M_2}\,\frac{\lambda_{12}}{\lambda_1} - \frac{15}{4A_{12}^*}\left(\frac{M_2-M_1}{2M_1}\right) - 1 ,$$

$$s^{(2)} = \frac{M_2+M_1}{2M_1}\,\frac{\lambda_{12}}{\lambda_2} - \frac{15}{4A_{12}^*}\left(\frac{M_1-M_2}{2M_2}\right) - 1 .$$

Choice of the correct sign for k_T requires some attention. When a mixture of gases with large heavy molecules and small light molecules is placed in a thermal gradient, the lighter molecules diffuse toward the warmer regions.[17] The concentration gradient, which is established by thermal diffusion, is opposed by ordinary mass diffusion which tends to equalize the composition, and, in time, a steady state is reached in which the opposing influences of thermal and ordinary diffusion balance. Then, ignoring pressure gradients, the concentration diffusion equation (2.29) becomes

$$\frac{\partial c}{\partial t} = D\left(\nabla^2 c + \frac{k_T}{T}\,\nabla^2 T\right) = 0 ,$$

where c is the mass concentration of the light gas (helium). Integration over an arbitrary volume of the mixture and use of Green's theorem to convert to a surface integral gives

$$\oint_s (\nabla c + (k_T/T)\nabla T)\cdot d\vec{s} = 0 ,$$

which implies

$$\nabla c = -(k_T/T)\,\nabla T .$$

Thus the thermal-diffusion ratio k_T must be negative so that the concentration of the light molecules increases as the temperature increases.

The values of the gas-transport coefficients and other relevant parameters for the gas mixtures were calculated with the use of a computer from the expressions presented in Appendices A and B. The calculations were made for the mixtures which were investigated experimentally. For the He-SF_6 mixtures, the partial pressure of SF_6 was 5 atm and the helium concentration was increased by adding helium. For the He-Xe mixtures, the Xe partial pressure was 8 atm. The values of the various transport coefficients for the pure gases are given in Table II, for the He-SF_6 mixtures in Table III and for the He-Xe mixtures in Table IV.

These values of the transport coefficients and gas parameters were then used to calculate the values of g_B, g_c, g_T shown in Figs. 3 and 5. The value of $g_{Bc_T}(\omega)$ was calculated for frequency shifts from 0 to 1200 MHz in increments of 5 MHz. The results are shown in Figs. 1 and 2.

The values of the gas parameters and transport

TABLE IV. Transport coefficients for He-Xe (8 atm) mixture.

He c'	He P lb/in.^{2}	$10^2\rho$ (g/cm^3)	$10^4\eta$ (g/cm sec)	$10^{-2}\lambda$ (erg/g sec °K)	$10^2 D$ (cm^2/sec)	$10^{-6} c_p$ (erg/g °K)	γ	$10^{-4} v_T$ (cm/sec)	Γ (MHz)
0	0	4.65	2.27	5.38	6.53	1.72	1.76	1.30	30.4
0.1	14	4.66	2.31	9.02	5.84	1.89	1.76	1.38	57.6
0.2	32	4.68	2.35	13.4	5.61	2.10	1.75	1.47	84.5
0.3	54	4.71	2.40	18.6	4.48	2.38	1.74	1.57	111
0.4	85	4.74	2.45	25.1	3.82	2.73	1.73	1.70	136
0.5	127	4.79	2.50	33.3	3.16	3.22	1.72	1.87	159
0.6	191	4.86	2.55	44.0	2.51	3.94	1.71	2.09	180
0.7	299	4.98	2.59	58.2	1.87	5.10	1.71	2.41	196
0.8	516	5.21	2.60	78.0	1.23	7.25	1.70	2.91	202
0.9	1183	5.92	2.49	107	0.600	12.7	1.69	3.96	175

coefficients which were calculated in this fashion were identical to the values used by Gornall *et al.*[19] Since these values were in excellent agreement with the spontaneous light-scattering spectra for the same mixtures as investigated in this experiment, we may assume the values are quite accurate, particularly for the mixtures with low-He concentration. For the mixtures with He concentration above 50%, the accuracy of the calculated values may be somewhat diminished due to the fact that the non-ideal-gas corrections and the effects of the He heavy-gas interactions become more important. Both of these effects are included in the calculations in an empirical fashion as discussed above.

---

†Research supported in part by the Office of Army Research, Durham, under Contract No. DAHC-04-68-C-0037.

*National Science Foundation Predoctoral Fellow. Present address: Laboratoire d'Optique Quantique, Bâtiment 503, Institut d'Optique, Faculté des Sciences, Orsay, France.

[1]V. I. Bespalov and A. M. Kubarev, Zh. Eksperim. i Teor. Fiz. Pis'ma v Redaktsiyu 6, 500 (1967) [Sov. Phys. JETP Letters 6, 31 (1967)].

[2]N. Bloembergen, W. H. Lowdermilk, M. Matsuoka, and C. S. Wang, Phys. Rev. A 3, 404 (1971).

[3]R. M. Herman and M. A. Gray, Phys. Rev. Letters 19, 824 (1967); D. H. Rank, C. W. Cho, N. D. Foltz, and T. A. Wiggins, *ibid.* 19, 828 (1967); T. A. Wiggins, C. W. Cho, D. R. Dietz, and N. D. Foltz, *ibid.* 20, 831 (1968).

[4]E. E. Hagenlocker, R. W. Minck, and W. G. Rado, Phys. Rev. 154, 226 (1967).

[5]I. M. Aref'ev and V. V. Morozov, Zh. Eksperim. i Teor. Fiz. Pis'ma v Redaktsiyu 9, 448 (1969) [Sov. Phys. JETP Letters 9, 269 (1969)].

[6]D. R. Dietz, C. W. Cho, D. H. Rank, and T. A. Wiggins, Appl. Opt. 8, 1248 (1969); C. W. Cho, C. J. Hsu, and N. D. Foltz, in Proceedings of the International Conference on Quantum Electronics, Kyoto, Japan, 1970, paper 19.5 (unpublished).

[7]N. Bloembergen, W. H. Lowdermilk, and C. S. Wang, Phys. Rev. Letters 25, 1476 (1970).

[8]L. D. Landau and E. M. Lifshitz, *Fluid Mechanics* (Addison-Wesley, Reading, Mass., 1958).

[9]L. D. Landau and E. M. Lifshitz, *Electrodynamics of Continuous Media* (Addison-Wesley, Reading, Mass., 1960).

[10]C. S. Wang, Phys. Rev. Letters 24, 1394 (1970).

[11]M. Kohler, Ann. Physik 39, 209 (1941).

[12]V. S. Starunov, Phys. Letters 26A, 428 (1968); Yu. P. Kyzylasov, V. S. Starunov, I. L. Fabelinskii, Zh. Eksperim. i Teor. Fiz. Pis'ma v Redaktsiyu 11, 110 (1970) [Sov. Phys. JETP Letters 11, 66 (1970)].

[13]P. C. Martin, in *Statistical Mechanics of Equilibrium and Non-Equilibrium*, edited by J. Meixner (North-Holland, Amsterdam, 1965), p. 124.

[14]R. D. Mountain and J. M. Deutch, J. Chem. Phys. 50, 1103 (1969).

[15]A. Dalgarno and A. E. Kingston, Proc. Roy. Soc. (London) A259, 424 (1960).

[16]Landolt-Börnstein, *Zahlenwerte und Funktionen*, 6th ed. (Springer, Berlin, 1959), Vol. II, Pt. 6, p. 873.

[17]S. Chapman and T. G. Cowling, *Mathematical Theory of Nonuniform Gases* (Cambridge U.P., Cambridge, England, 1970).

[18]J. O. Hirschfelder, C. F. Curtiss, and R. B. Bird, *The Molecular Theory of Gases and Liquids* (Wiley, New York, 1954).

[19]W. S. Gornall, C. S. Wang, C. C. Young, and N. Bloembergen, Phys. Rev. Letters 26, 1094 (1971).

[20]W. S. Gornall and C. S. Wang, J. Phys. (Paris) (to be published).

[21]M. Denariez and G. Bret, Phys. Rev. 171, 160 (1968).

[22]G. I. A. Stegeman and B. P. Stoicheff, Phys. Rev. Letters 21, 202 (1968).

[23]M. Born and E. Wolf, *Principles of Optics*, 3rd ed. (Pergamon, New York, 1965).

[24]N. M. Kroll, J. Appl. Phys. 36, 34 (1965); R. L. Carman, F. Shimizu, C. S. Wang, and N. Bloembergen, Phys. Rev. A 2, 60 (1970); N. M. Kroll and P. L. Kelley, *ibid.* 4, 763 (1971).

[25]H. T. Buscher, R. G. Tomlinson, and E. K. Damon, Phys. Rev. Letters 15, 847 (1965).

[26]N. F. Sather and J. S. Dahler, J. Chem. Phys. 35, 2029 (1961).

[27]R. Holmes and M. A. Stott, Brit. J. Appl. Phys. 1, 1331 (1968).

[28]C. L. O'Connor, J. Acoust. Soc. Am. 26, 361 (1954).

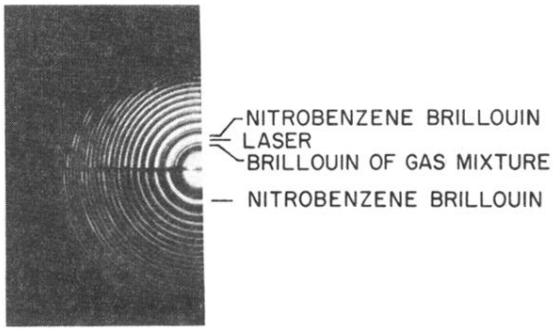

FIG. 10. Interference fringes showing spectral characteristics of light at the backward traveling input of the gas cell (lower part) and the output after stimulated backward gain (upper part). The spacing of the FP plates was 6 cm.

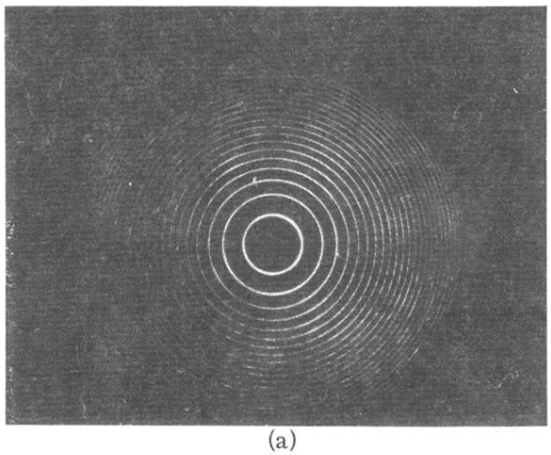

(a)

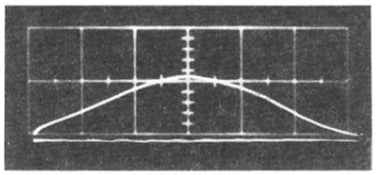

(b)

FIG. 7. (a) Frequency content of ruby laser pulse analyzed by a 6-cm Fabry-Perot etalon. (b) Oscilloscope trace of laser power output (horizontal scale: 20 nsec/div).